PERFORMANCE ANALYSIS OF DISPERSED SPECTRUM COGNITIVE RADIO SYSTEMS

A Thesis

by

MUNEER MOHAMMAD

Submitted to the Office of Graduate Studies of
Texas A&M University
in partial fulfillment of the requirements for the degree of

MASTER OF SCIENCE

December 2009

Major Subject: Electrical Engineering

PERFORMANCE ANALYSIS OF DISPERSED SPECTRUM COGNITIVE RADIO SYSTEMS

A Thesis

by

MUNEER MOHAMMAD

Submitted to the Office of Graduate Studies of
Texas A&M University
in partial fulfillment of the requirements for the degree of

MASTER OF SCIENCE

Approved by:

Chair of Committee,	Erchin Serpedin
Committee Members,	Khalid Qaraqe
	Jose Silva-Martinez
	Donald Friesen
Head of Department,	Costas Georghiades

December 2009

Major Subject: Electrical Engineering

ABSTRACT

Performance Analysis of Dispersed Spectrum Cognitive Radio Systems.

(December 2009)

Muneer Mohammad, B.S., Jordan University of Science and Technology

Chair of Advisory Committee: Dr. Erchin Serpedin

Dispersed spectrum cognitive radio systems represent a promising approach to exploit the utilization of spectral resources to full extent. Therefore, the performance analysis of such systems is conducted in this research. The average symbol error probability of dispersed spectrum cognitive radio systems is derived for two cases: where each channel realization experiences independent and dependent Nakagami-m fading, respectively. In addition, the derivation is extended to include the effects of modulation type and order by considering M-PSK and M-QAM modulation schemes. We then study the impacts of topology on the effective transport capacity performance of ad hoc dispersed spectrum cognitive radio systems where the nodes assume 3- dimensional (3D) configurations. We derive the effective transport capacity considering a cubic grid distribution. In addition, numerical results are presented to demonstrate the effects of topology on the effective transport capacity of ad hoc dispersed cognitive radio systems.

.

DEDICATION

To my parents, brothers and sister

ACKNOWLEDGEMENTS

First of all, I can never be thankful enough to God who has provided me with health, life, and guidance. All praise and gratitude belong to Him.

My sincerest gratitude and thanks go to my advisors, Dr. Khalid Qaraqe and Dr. Hasari Celebi, who provided me with the opportunity and environment to carry out my research. Their constant support and guidance throughout my research have strengthened me as a researcher. I am also very grateful for the level of freedom they have allowed me in conducting my research.

Third, my gratitude goes to my research committee, Erchin Serpedin, Donald Friesen, and Jose-Silva, for their time, support, and encouragement. I also thank the Department of Electrical and Computer Engineering at Texas A&M University and the administrative staff for creating a supportive environment.

My deepest gratitude goes to my family for their constant support and unconditional love. They have provided me with the support I needed to survive the darker days of research. I am particularly thankful to my cousin, Dr. Eyad Masad, who made me feel better every time I talked to him.

I would like to thank my friends in College Station for many happy memories. My appreciation goes out to Dr. Wael, Nathan, Rakan, Joshua and all friends in College Station. I am also very thankful to my friends Saleh and Ahmad in Jordan. Special thanks to my uncle, Ziad Masad and my brothers, Mohammad, Manar, Murad, Majdi, and Muntaser.

TABLE OF CONTENTS

Page

LIST OF FIGURES

FIGURE Page

FIGURE Page

LIST OF TABLES

1. INTRODUCTION

1.1 Motivations

Cognitive radio is a new approach to develop intelligent and sophisticated wireless systems [1], which can require utilization of spectral resources dynamically. Cognitive radio systems that employ the dispersed spectrum utilizations as spectrum access method is called dispersed spectrum cognitive radio systems [2]. In dispersed spectrum cognitive radio systems, information can be transmitted mainly using two approaches. In the first approach, information (or signal) is splitted into k data streams and these data streams are transmitted over k available frequency bands as shown in Fig.1. In the second approach, information (or signal) is replicated k times and each copy is transmitted over one of the available k bands. The second approach is illustrated in Fig. 2. Note that the second approach is considered in this study.

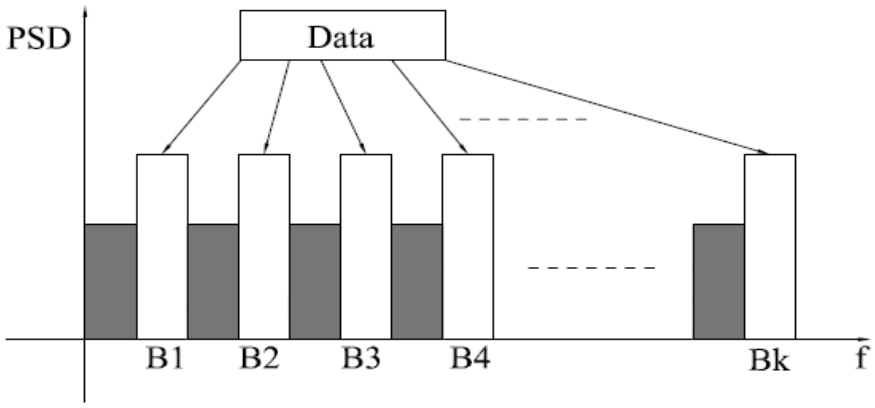

Fig. 1 Illustration of dispersed spectrum utilization of the first approach.

This thesis follows the style of *IEEE Transactions on Wireless Communications.*

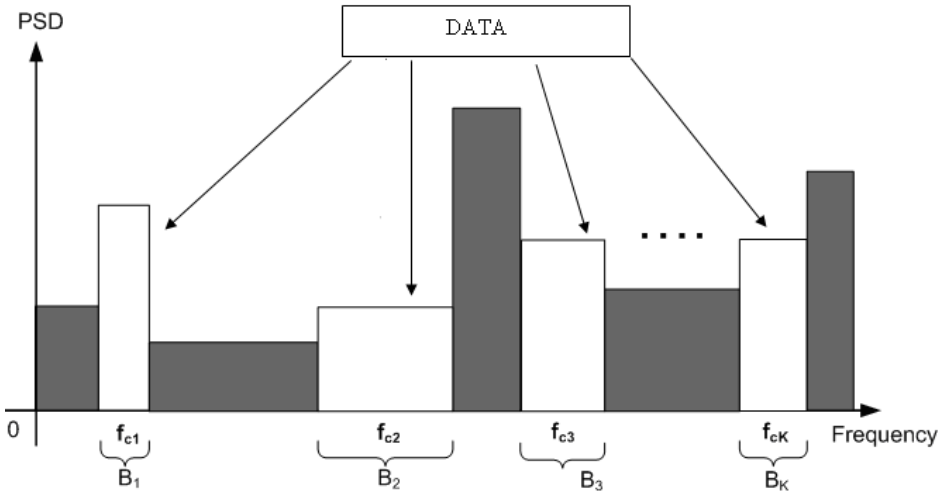

Fig. 2 Illustration of dispersed spectrum utilization of the second approach.

Theoretical limits for the time delay estimation problem in dispersed spectrum cognitive radio systems are investigated in [2]. In this study, Cramer-Rao Lower Bounds (CRLBs) for known and unknown carrier frequency offset (CFO) are derived and the effects of the number of available dispersed bands and modulation schemes on the CRLBs are investigated. In addition, the idea of dispersed spectrum cognitive radio is applied to UWB communications systems in [3]. Moreover, the performance comparison of whole and dispersed spectrum utilization methods for cognitive radio systems is studied in the context of time delay estimation in [4]. In these prior works, dispersed spectrum cognitive radio systems are investigated for localization and positioning applications. More importantly, it is assumed that all channels in such systems are assumed to be independent from each other. In addition, single- path flat fading channels

are assumed in the prior works. However, in realistic scenarios, the channels are not single-path flat fading channels and they may not be independent from each other.

In this research, the performance analysis of dispersed spectrum cognitive radio systems is conducted in the context of communications applications and symbol error probability is used as the performance metric. Average symbol error probability is derived under two conditions, i.e., the scenarios when each channel experiences independent and dependent Nakagami-m fading. The derivation for both cases is extended to include the effects of modulation type and order, namely M-QAM, M-PSK for M=4 and 16. The effect of convolutional coding on the symbol error probability is also investigated through computer simulations. Finally, numerical results are provided to study the performance of dispersed spectrum cognitive radio systems for different fading conditions, modulation, and coding schemes.

In [5,6], the authors represent a new communication model, namely the square configuration (2D), to reduce the inter-node interference and study the impact of different types of modulations over AWGN and Rayleigh fading channels on the effective transport capacity. Moreover in [5, 6, 7, 8], it is assumed that the nodes assume a square distribution 2- dimensional configuration. This study also assumes that each node is centered inside of a cube located at the vertices of cubic grid in a spherical volume V which represents a 3- dimensional configuration (3D). When the nodes are distributed in three dimensions, it will decrease the effects of the inter node interference, thus increasing the effective transport capacity. In fact, the 3D-configuration is more practical than the previous one. One of the most useful applications for this configuration is in network sensors [9].

In this study, the performance analysis of ad hoc dispersed spectrum cognitive radio systems is conducted. The effects of node distribution on the effective transport capacity of ad hoc dispersed spectrum cognitive radio systems are investigated. The effective transport capacity is derived considering a 3-D node distribution. Finally, numerical results are provided to verify the theoretical analysis.

This study deals with dispersed spectrum cognitive radio systems [7] when M-QAM and M-PSK are in use over the Nakagami-m fading channel. This study includes two cases: Independent and dependent channel realizations, where each channel realization is independent or dependent from each other. The channel diversity is due to the fact that each node sends a replicate data over multiple carrier frequencies to the next node. In this case the performance will be improved in terms of error probability, which leads to enhanced effective transport capacity.

1.2 System Model

In wireless communication systems, the modulated signal is transmitted through the fading channels. Each channel realization exhibits a specific time varying gain and propagation delay as well, and is characterized by the impulse response

$$h(t,\tau)=\sum_{i=1}\alpha_i(t)\delta(\tau-\tau_i(t))e^{-j\varphi_i(t)}\,, \tag{1.1}$$

where $\{\alpha_i(t)\},\{\tau_i(t)\}$ and $\{\varphi_i(t)\}$ are the random time varying path gain, propagation delay and phase sequences, respectively, and $\delta(\cdot)$ is the delta function. The time invariant version of this model is suggested by [4] to describe multi-path stationary fading channels and is defined as

$$h(\tau)=\sum_{i}\alpha_i\delta(\tau-\tau_i)e^{-j\varphi_i}\,. \tag{1.2}$$

A modulated signal waveform with carrier frequency f_c can be expressed as

$$s(t) = \Re\left\{\tilde{s}(t)e^{j2\pi f_c t}\right\}, \tag{1.3}$$

where f_c is the carrier frequency, and $\tilde{s}(t)$ represents the equivalent low-pass waveform of the transmitted signal.

For the k dispersed bands in Fig.2, the modulated signal waveform of the i^{th} band can be expressed as

$$s_i(t) = \Re\left\{\tilde{s}(t)e^{j2\pi f_{ci} t}\right\} . \tag{1.4}$$

Assuming that the modulated signal is transmitted over a mobile radio fading channel with K diversity bands and assuming that the channel at the i^{th} band is characterized by an equivalent low-pass impulse as

$$h_i(\tau) = \sum_{l=1}^{L} \alpha_{i,l}\delta\left(\tau - \tau_{i,l}\right)e^{-j\varphi i,l}, \tag{1.5}$$

where $\alpha_{i,l}$, $\tau_{i,l}$ and $\varphi_{i,l}$, are the parameters showing the path gain, propagation delay, and phase of the l^{th} path at i^{th} band, respectively. Slow and non-selective fading on each diversity channel and the K diversity over Nakagami-m distribution envelope statistics with different values of m and different transmitted power and noise are also assumed. The transmitted signal carried over each band is independently corrupted by an additive white Gaussian noise process, then all received signals passed through Maximum Ratio Combing (MRC) as shown in Fig. 3.

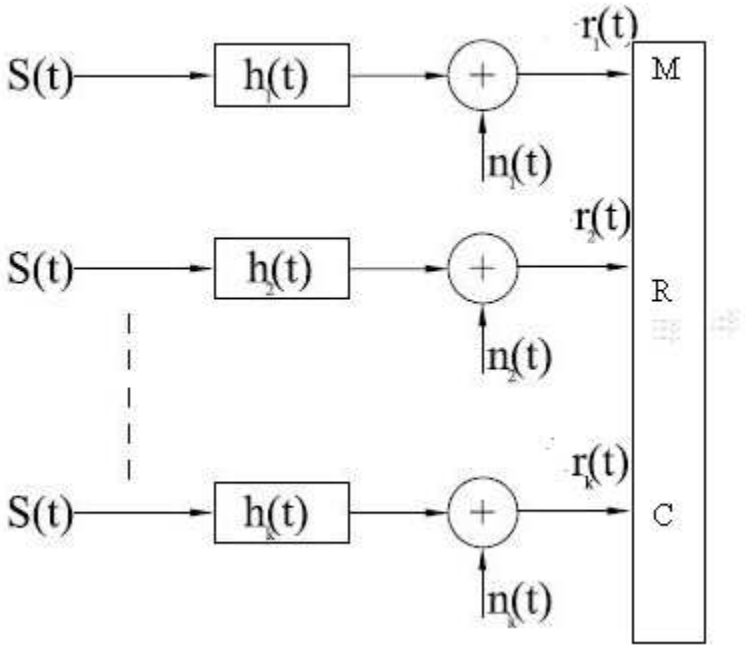

Fig. 3 System model for dispersed spectrum cognitive radio systems.

In the receiver, the signal passed through to bandpass filter (BPF) and downconverted to a baseband signal at each band.

In the baseband model, the received signal for the i^{th} band can be expressed as

$$r_i(t) = \sum_{l=1}^{L} \alpha_{i,l} s_i\left(t - \tau_{i,l}\right) e^{-j\varphi_{i,l}} + n_i(t) \quad , \tag{1.6}$$

where $n_i(t)$ is a zero mean complex-valued white Gaussian noise process with power spectral density N_O.

We define the total signal to noise ratio (γ_{Tot}) as

$$\gamma_{Tot} = \sum_{i=1}^{K} \gamma_i \quad , \tag{1.7}$$

where γ_i is the SNR at the i^{th} branch. Assuming that the received power from the i^{th} band is equal to ($\alpha_i p$) and the AWGN experienced in this band has a power spectral density of ($\beta_i N_0$). The total SNR can be expressed as

$$\gamma_{Tot} = \gamma_1 + \sum_{i=2}^{K} \frac{\alpha_i}{\beta_i} \gamma_1 = \gamma_1 + \sum_{i=2}^{K} k_i \gamma \ , \tag{1.8}$$

where $\gamma_1 = \frac{P}{No}$ and $k_i = \frac{\alpha_i}{\beta_i}$

The Probability Density Function (PDF) of Gaussian is given by

$$p_{n_i}(x) = \frac{1}{\sqrt{2\pi}\sigma_i} \exp\left(-\frac{x^2}{2\sigma_i^2} \right) \ , \tag{1.9}$$

$$p_{r_i}(R_i) = p_{n_i}\left(r_i(t) - \alpha_i e^{-j2\pi f_{ci} t} s_i(t-\tau) \right) = \frac{1}{\sqrt{2\pi}\sigma_i} \exp\left(-\frac{\left(r_i(t) - \alpha_i e^{-j2\pi f_{ci} t} s_i(t-\tau) \right)^2}{2\sigma_i^2} \right) , \tag{1.10}$$

$$\begin{aligned} p_{r_i}(R) &= \prod_{i=1}^{K} p_{n_i}\left(r_i(t) - \alpha_i e^{-j2\pi f_{ci} t} s_i(t-\tau) \right) \\ &= \left(\prod_{i=1}^{K} \frac{1}{\sqrt{2\pi}\sigma_i} \right) . \exp\left(-\sum_{i=1}^{K} \frac{\left(r_i(t) - \alpha_i e^{-j2\pi f_{ci}} s_i(t-\tau) \right)^2}{2\sigma_i^2} \right) \end{aligned} \ , \tag{1.11}$$

By taking the logarithm, we will get.

$$Log\left(p_r(R) \right) = Log\left(\prod_{i=1}^{K} \frac{1}{\sqrt{2\pi}\sigma_i} \right) - \left(\sum_{i=1}^{K} \frac{\left(r_i(t) - \alpha_i e^{-j2\pi f_{ci} t} s_i(t-\tau) \right)^2}{2\sigma_i^2} \right) \ . \tag{1.12}$$

From (1.12), assuming that the value between $\left| \ \right|$ is y, it follows that:

$$-|y|^2 = -yy^* = -|r_i(t)|^2 + r_i(t)\alpha_i e^{-j2\pi f_c t} s_i(t-\tau) + r_i(t)\alpha_i e^{j2\pi f_{ci} t} s_i(t-\tau) - |\alpha_i|^2 |s_i(t-\tau)|^2 \tag{1.13}$$

$$= -|r_i(t)|^2 + r_i(t)\alpha_i e^{-j2\pi f_c t} s_i(t-\tau) + r_i(t)\alpha_i e^{j2\pi f_{ci} t} s_i(t-\tau) - |\alpha_i|^2 |s_i(t-\tau)|^2 \ , \tag{1.14}$$

.

Thus,

$$-|y|^2 = 2\Re\left\{r_i^*(t)\alpha_i e^{j2\pi f_{ci}t} s_i(t-\tau)\right\} - |\alpha_i|^2 |s_i(t-\tau)|^2 \quad . \qquad (1.15)$$

1.3 Derivation of the Probability of Error for M-QAM

By looking at the signal constellation in Fig. 3, it can be easily seen that there are three types of decision regions:

- The decision regions of the red points. The number of these regions is equal to 4.
- The decision regions of the green points. The number of these regions is equal to $4.\left(\sqrt{M}-2\right)$.
- The decision regions of the black points. The number of these regions is equal to $\left(\sqrt{M}-2\right)^2$.

The noise presents the horizontal-inphase (n_1) and vertical-quadrature (n_2) components.

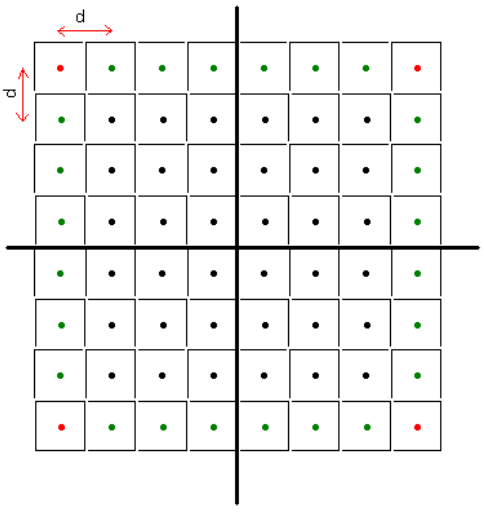

Fig. 4 Signal constellation for M-QAM.

We will find the probability of correct decision, and then find the probability of error.

1. The first region

$$p(c/region-1)=pr\left\{n_1<\frac{d}{2}\ \&\ n_2<\frac{d}{2}\right\}=pr\left\{n_1<\frac{d}{2}\right\}pr\left\{n_2<\frac{d}{2}\right\}=\left(pr\left\{n<\frac{d}{2}\right\}\right)^2$$
$$=\left(\frac{1}{\sqrt{\pi N_0}}\int_{-\infty}^{d/2}\exp\left\{\frac{-x^2}{N_0}\right\}dx\right)^2=(1-p)^2,\ where\qquad p=Q\left(\frac{d}{\sqrt{2N_0}}\right) \tag{1.16}$$

2. The second region

$$p(c/region-2)=pr\left\{\frac{-d}{2}<n_1<\frac{d}{2}\ \&\ n_2<\frac{d}{2}\right\}=pr\left\{\frac{-d}{2}<n_1<\frac{d}{2}\right\}pr\left\{n_2<\frac{d}{2}\right\}$$
$$=\frac{1}{\pi N_0}\int_{-d/2}^{d/2}\exp\left\{\frac{-x^2}{N_0}\right\}dx\int_{-\infty}^{d/2}\exp\left\{\frac{-y^2}{N_0}\right\}dy=(1-2p)(1-p) \tag{1.17}$$

3. The third region

$$p(c/region-3)=pr\left\{\frac{-d}{2}<n_1<\frac{d}{2}\ \&\ \frac{-d}{2}<n_2<\frac{d}{2}\right\}=\left(pr\left\{\frac{-d}{2}<n<\frac{d}{2}\right\}\right)^2$$
$$=\left(\frac{1}{\sqrt{\pi N_0}}\int_{-d/2}^{d/2}\exp\left\{\frac{-x^2}{N_0}\right\}dx\right)^2=(1-2p)^2 \tag{1.18}$$

For $p(s_i)=\frac{1}{M}, i=1,2,\ldots,M$, the probability of correct decision can be expressed as:

$$p(c)=\sum_{i=1}^{M}p(c/s_i)p(s_i)=\frac{1}{M}\sum_{i=1}^{M}p(c/s_i)$$
$$=\frac{1}{M}\left\{4(1-p)^2+4\left(\sqrt{M}-2\right)(1-2p)(1-p)+\left(\sqrt{M}-2\right)^2(1-2p)^2\right\} \tag{1.19}$$
$$=\frac{1}{M}\left\{M+\left(4\sqrt{M}-4M\right)p+\left(4-8\sqrt{M}+4M\right)p^2\right\}$$

And after some manipulation, the probability of correct decision can be expressed as:

$$p(c)=\left(1-2\left(1-\frac{1}{\sqrt{M}}\right)p\right)^2 \quad . \tag{1.20}$$

Knowing from [10] that $p = Q\left(\frac{d}{\sqrt{2N_0}}\right)$, and $d = 2\sqrt{E_0}$, and substituting d into the equation of the probability of correct decision (), we obtain the following expression:

$$p(c) = \left(1 - 2\left(1 - \frac{1}{\sqrt{M}}\right)Q\left(\sqrt{\frac{3E_{av}}{(M-1)N_0}}\right)\right)^2 \quad . \tag{1.21}$$

Note that, the probability of error is defined as

$$P_e = 1 - p(c) \quad . \tag{1.22}$$

The bit error probability is obtained as defined as in [11]

$$Pe = 1 - \left[1 - \left(2\left(1 - \frac{1}{\sqrt{M}}\right)Q\left(\sqrt{\frac{3\log_2 M}{M-1}\frac{E_{av}}{N_0}}\right)\right)\right]^2 \quad . \tag{1.23}$$

2. AVERAGE SYMBOL ERROR PROBABILITY FOR INDEPENDENT CHANNELS

In this section, we study the performance of digital modulation techniques: M-QAM and M-PSK over AWGN channels and flat fading channels. In this study, we focus on a Nakagami-m fading channel to study the performance of the dispersed spectrum cognitive radio system for M-QAM and M-PSK under different severity parameters m and different conditions of the fading channel.

2.1 Additive White Gaussian Noise (AWGN) Channel

The additive white Gaussian noise is present in all channels. We study the performance of a dispersed cognitive radio system in the ideal case where the channels are experiencing different AWGNs for two types of modulations namely, M-QAM and M-PSK

A. M-QAM

The probability of error for a rectangular M-QAM is given in [11] as:

$$Ps = 1 - \left[1 - \left(2\left(1 - \frac{1}{\sqrt{M}}\right)Q\left(\sqrt{\frac{3}{M-1}\frac{E_{av}}{N_0}}\right)\right)\right]^2 \quad , \tag{2.1}$$

Where E_{av}/N_0 is the average SNR per symbol and is equal to $(LogM)E_b/N_0$, where E_b/N_0 is the average SNR per bit.

From the definition of SNR as stated in (1.15), we can rewrite (2.1) as

$$Ps = 1 - \left[1 - \left(2\left(1 - \frac{1}{\sqrt{M}}\right)Q\left(\sqrt{\frac{3.\gamma_{equ}}{M-1}}\right)\right)\right]^2 . \tag{2.2}$$

The idea of using k-bands is that each band has different carrier frequency, power, and noise. These parameters have effect on the performance in terms of error probability as shown in Figs. 4 and 5.

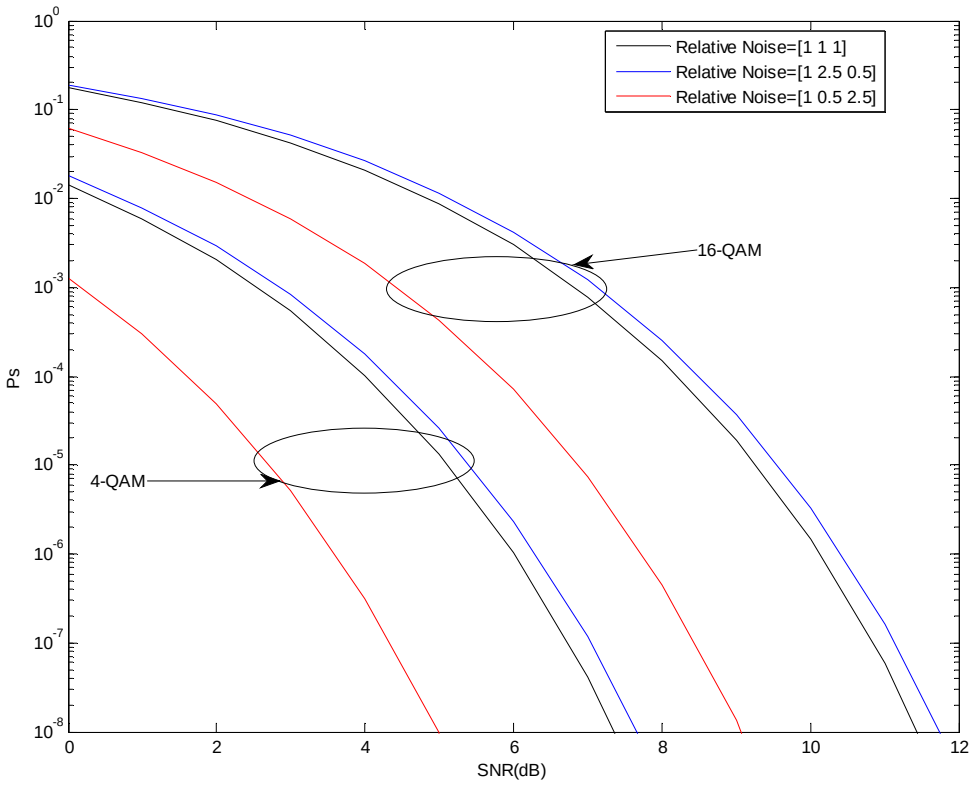

Fig. 5 Average symbol error probability versus average SNR per bit per first branch for (16 and 4) QAM signals for three diversity branches with RP= [1 2 0.5].

In Fig. 5, each curve represents the symbol error probability versus SNR when using three bands where each band experiences different power and noise. Relative noise Relative Noise (RNo) and Relative Power (RP) represent the relative noise and relative power, respectively, with respect to the first branch. For example, when saying RP= 1 2 0.5 , it means that the second band has power equal twice the first band, and the power transmitted in the second band is 0.5 of the power transmitted in the first band. Such a

relationship among the power levels of different branches is referred to as unbalanced branches. The scope of this figure is to show the importance of the power and noise in each band. The blue and red curves experience the same noise but as seen in Fig. 4 the performance of the red curve is much better than the blue one, since the power in the red curve is distributed in the sense that the larger power on the band presents the noise with lower power, and the SNR for the 3-bands is calculated based on combining the SNR on each band. In conclusion, we can note that the system performs better when the branches present the highest received power.

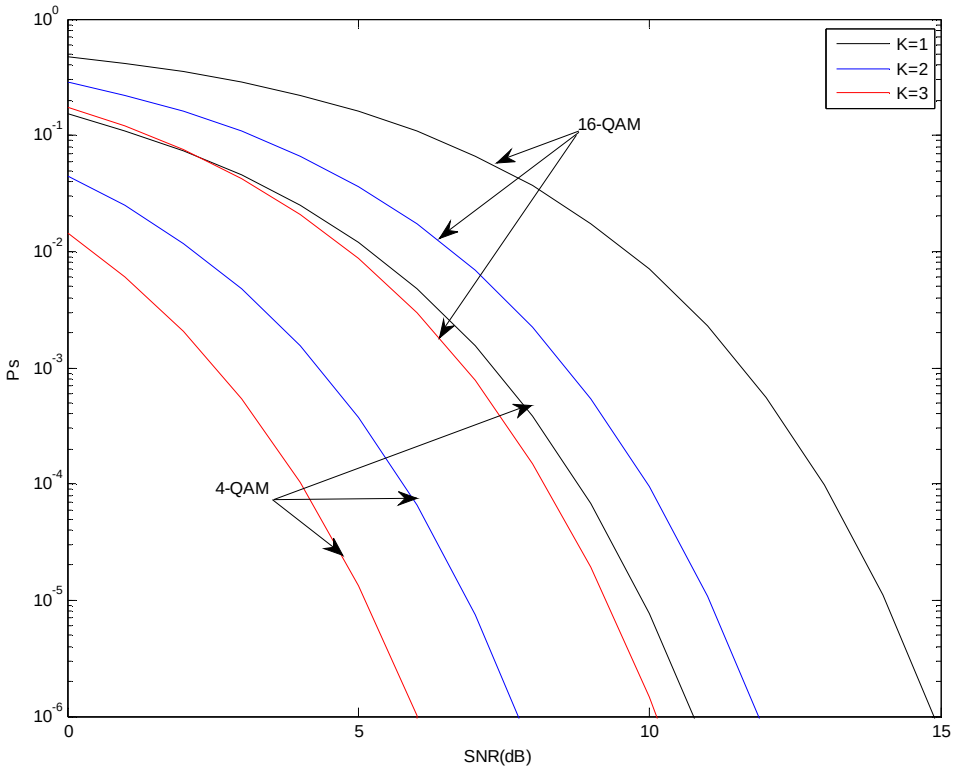

Fig. 6 Average symbol error probability versus average SNR per bit per first branch for (16- and 4-) QAM signals with k=1,2,3.

Fig. 6 illustrates the effect of diversity order on the symbol error probability performance of the system and we can see that as the diversity order increases, the performance is improved.

B. M-PSK

In this study, we are going to focus on 16-PSK. The exact symbol average error probability is given in [12] as

$$P_S = \frac{1}{\pi}\int \exp\left(\frac{-g_{psk}\,\gamma_{Tot}}{\sin^2\phi}\right)d\phi\ , \tag{2.6}$$

where $g_{psk} = \sin^2\left(\frac{\pi}{M}\right)$. 2.7)

1. Unbalanced branches

When all bands have the different power and spectral noise, SNR is defined as

$$\gamma_{Tot} = \gamma_1 + \sum_{i=2}^{K}\frac{\alpha_i}{\beta_i}\gamma = \gamma_1 + \sum_{i=2}^{K} k_i\gamma$$

We then can re-write (2.6) as

$$P_s = \frac{1}{\pi}\int_0^{(M-1)\frac{\pi}{M}} \exp\left(\frac{-g_{psk}\left(\gamma + \sum_{i=2}^{K} k_i.\gamma\right)}{\sin^2\phi}\right)d\phi \quad . \tag{2.8}$$

2. Balanced branches

When all bands have the same power and spectral noise we can re-write (1.8)

as $\gamma_{Tot} = K\gamma$, (2.9)

So, (2.8) is going to be

$$P_s = \frac{1}{\pi}\int_0^{(M-1)\frac{\pi}{M}} \exp\left(\frac{-g_{psk}(k.\gamma)}{\sin^2\phi}\right)d\phi. \tag{2.10}$$

2.2 Fading Channels

In fading channels, the transmitted signal varies with distance and is subject to the time delay due to existence of the multipath fading channel. We consider two types of fading channels, namely Nakagami-m fading channels and Rayleigh fading channels.

2.2.1 Rayleigh Fading Channels

A. M-QAM

Assume that the signals are transmitted over i.i.d Rayleigh fading channels. The next equation is derived in [5].

$$P_S = \int_0^{\infty} P_S(\gamma) P_{\gamma s}(\gamma) d\gamma , \tag{2.11}$$

$$= \frac{4}{\pi}\left(1 - \frac{1}{\sqrt{M}}\right)\int_0^{\pi/2} \mu_{\gamma s}\left(-\frac{g}{\sin^2 \phi}\right) d\phi - \frac{4}{\pi}\left(1 - \frac{1}{\sqrt{M}}\right)^2 \int_0^{\pi/4} \mu_{\gamma s}\left(-\frac{g}{\sin^2 \phi}\right) d\phi , \tag{2.12}$$

where the MGF (Moment generating Function) is defined as follows

$$\mu_{\gamma s_{Tot}} = \left(1 + s\,\bar{\gamma}_{equ}\right)^{-K} , \tag{2.13}$$

and g is a function of the size of M-QAM constellation, and is defined as

$$g = \frac{1.5}{M - 1} . \tag{2.14}$$

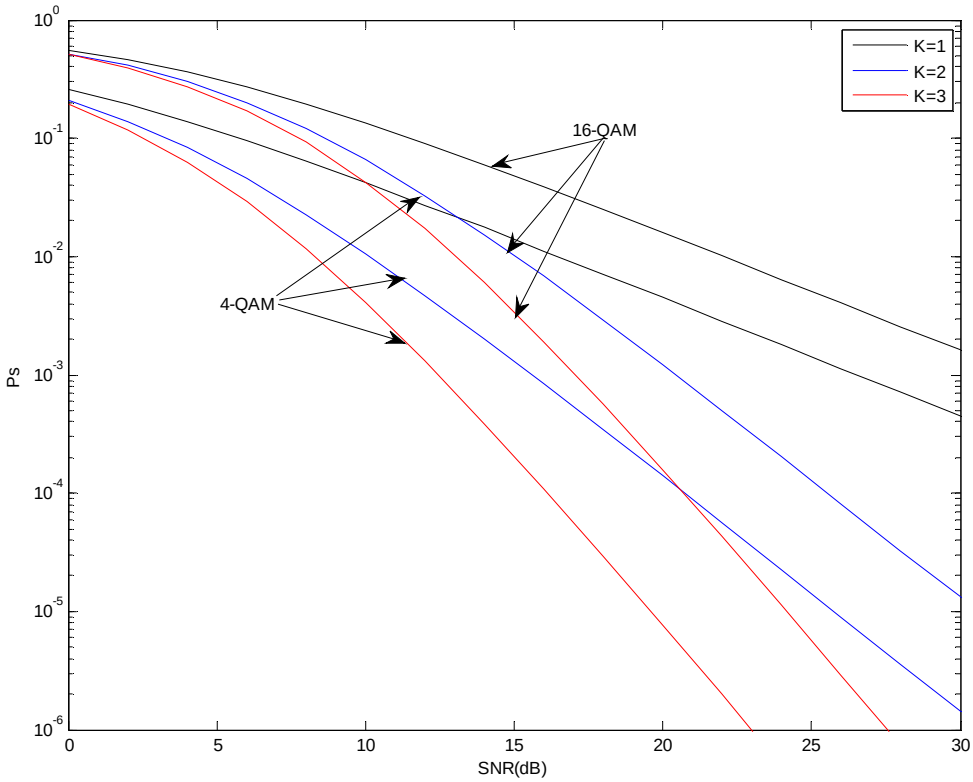

Fig.7 Average symbol error probability versus average SNR per bit per first branch for (16- and 4-) QAM signals with k=1,2,3 (Rayleigh channels).

Fig. 7 illustrates the effect of diversity levels on the probability performance for coherent detection of (4- and16-) QAM signals under Rayleigh fading channels. It can be shown that increasing the diversity order improves the performance of the system and it becomes closer to the performance achieved in an AWGN.

B. M-PSK

The Moment Generator Function is defined in (2.13) as

$$\mu_{\gamma s_{-tot}} = \left(1 + s\,\gamma_{Tot}\right)^{-1} \quad . \tag{2.15}$$

The MGF for K-bands is defined as

$$\mu_{\gamma_{S-tot}} = \left(1 + \frac{g\ \gamma_{Tot}}{\sin^2 \phi}\right)^{-K} \tag{2.16}$$

1. Unbalanced Branches

As in (1.8), SNR is defined as $\gamma_{Tot} = \gamma_1 + \sum_{i=2}^{K} \frac{\alpha_i}{\beta_i} \gamma = \gamma_1 + \sum_{i=2}^{K} k_i \gamma$

So, we can rewrite (2.7) as

$$\mu_\gamma = \prod_{i=1}^{k} \left(1 + \frac{g\gamma_i}{\sin^2 \phi}\right)^{-i} = \mu_\gamma = \prod_{i=1}^{k} \left(1 + \frac{g \frac{k_i}{\sum_{i=1}^{k} k_i}}{\sin^2 \phi}\right)^{-i} \quad . \tag{2.17}$$

2. Balanced Branches

Gamma's in all bands are equal, implying that $\gamma_{Tot} = k\gamma$

So, we can rewrite (2.7) as

$$\mu_\gamma = \prod_{i=1}^{k} \left(1 + \frac{g.k.\gamma}{\sin^2 \phi}\right)^{-i} = \left(1 + \frac{g.k.\gamma}{\sin^2 \phi}\right)^{-k} \quad . \tag{2.18}$$

2.2.2 Nakagami-m Fading Channel

This type of fading channel is a general case for Rayleigh fading channels, since the severity fading channel parameter (m) can take values from 0.5 to ∞. The case when m=1 reduces to the Rayleigh fading channel, and when m=∞, it simplifies to an AWGN channel.

We utilize the Moment Generator Function (MGF) technique to find an expression for the average probability of error for M-QAM, and M-PSK modulations in Nakagami-m fading.

A. M-QAM

The average symbol error probability is obtained by averaging the error probability for AWGN over a Nakagamai-m fading distribution channel which is defined in (2.11) as

$$P_S = \int_0^{\infty} P_S(\gamma) P_{\gamma s}(\gamma) d\gamma$$

$$= \frac{4}{\pi}\left(1 - \frac{1}{\sqrt{M}}\right)\int_0^{\pi/2} \mu_{\gamma s}\left(-\frac{g}{\sin^2 \phi}\right) d\phi - \frac{4}{\pi}\left(1 - \frac{1}{\sqrt{M}}\right)^2 \int_0^{\pi/4} \mu_{\gamma s}\left(-\frac{g}{\sin^2 \phi}\right) d\phi \quad , \quad (2.19)$$

where $\mu_{\gamma s_{-tot}}\left(-\frac{g}{\sin^2 \phi}\right) = \left(1 + \frac{g\gamma_s}{mk \sin^2 \phi}\right)^{-mk}$, (2.20)

where g is a function of the size of M-QAM, being defined as $g = \frac{1.5}{M - 1}$.

- Case 1: Pot of the average symbol error probability versus average SNR per bit for (4- and 16-) QAM signals with k=1, Nakagami-m fading channel for different values of m.

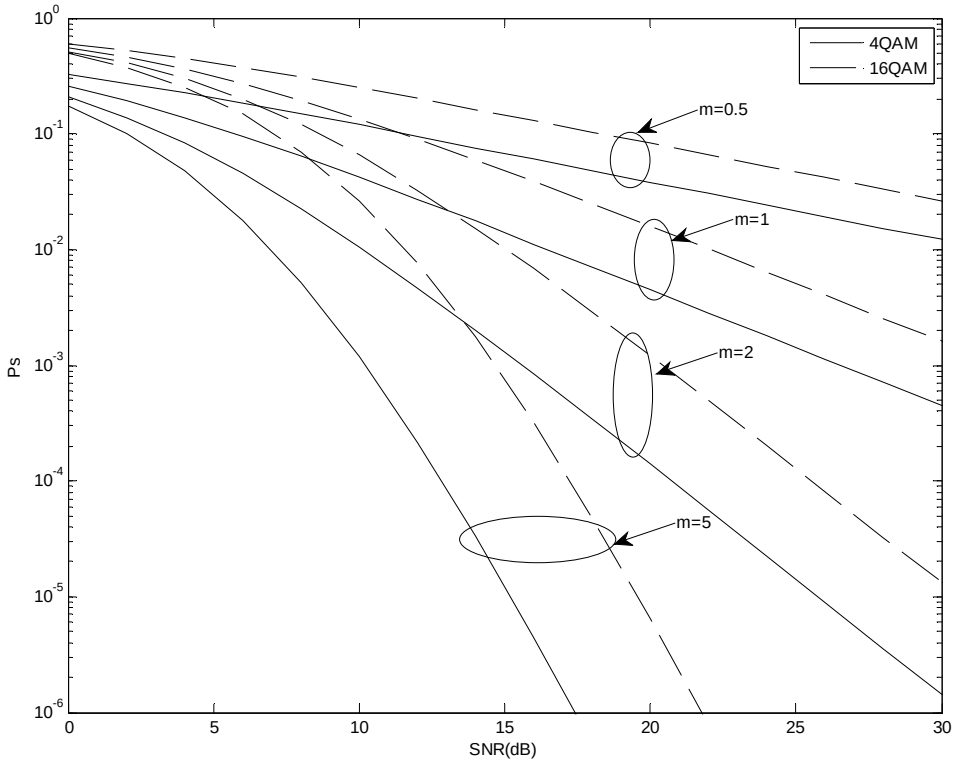

Fig. 8 Average symbol error probability versus average SNR per bit per first branch for (16- and 4-) QAM signals with k=1, Nakagami-m channel.

Fig. 8 illustrates the effect of the fading severity parameter on error probability performance and it can be seen that the system performs better under less severity (m increased).

- Case 2: Study the influence of the fading severity parameters where three branches with different severity parameters are used.

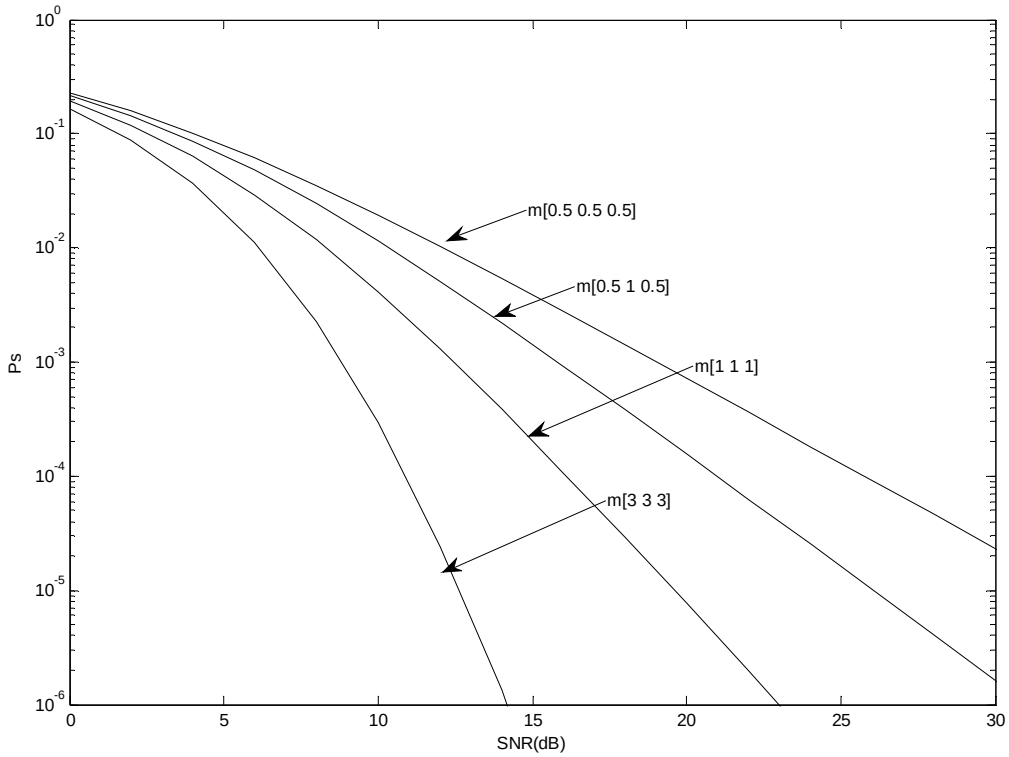

Fig. 9 Average symbol error probability versus average SNR per bit per firstbranch for 4-QAM signals with k=3, Nakagami-m fading channels with different fading-severity parameters.

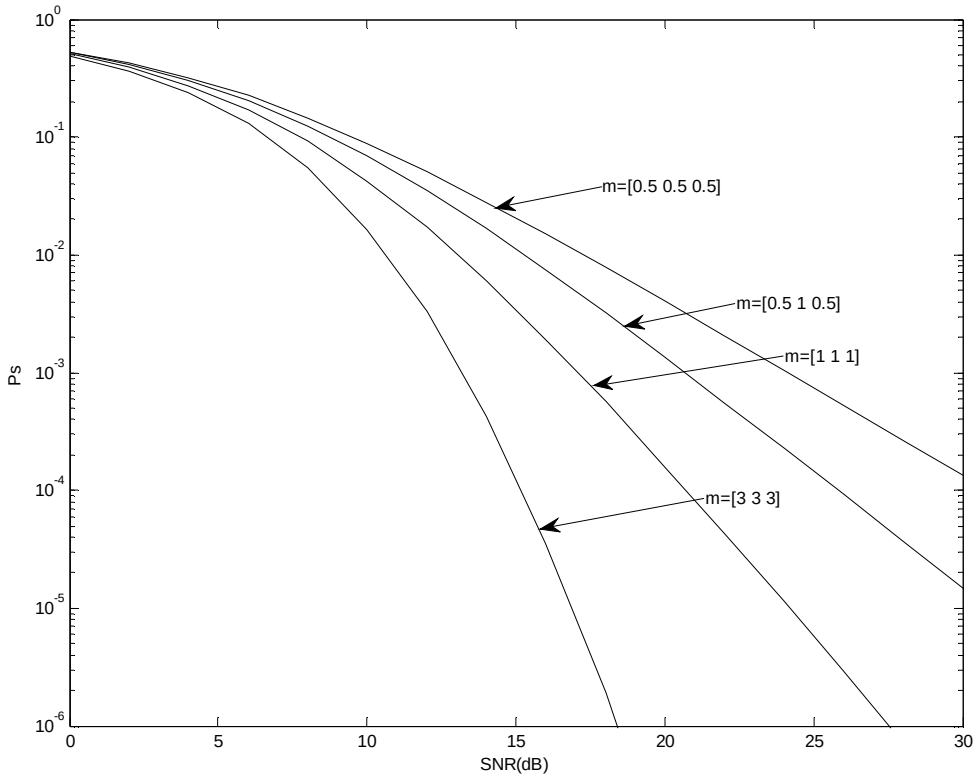

Fig. 10 Average symbol error probability versus average SNR per bit per first branch for 16-QAM signals with k=3, Nakagami-m fading channels with different fading-severity parameters.

The influence of the fading severity parameters is also studied in the Figs. 9 and 10 where three branches with different severity parameters are used. The system performs better when the branches have lowest severity parameters m.

- Case 3: The effect of unbalanced diversity branches on the error probability performance.

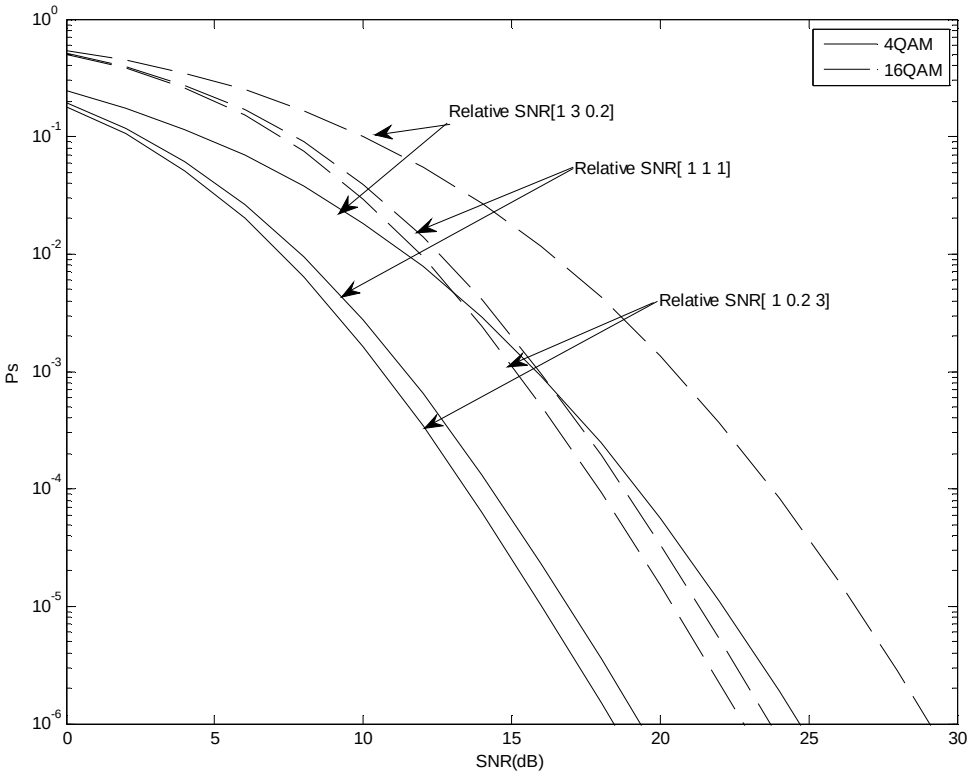

Fig. 11 Average symbol error probability versus average SNR per bit for (16- and 4-) QAM signals with 3 unbalanced diversity branches with m=1, 0.5,3 for k=1, 2, 3, respectively.

Fig.11 studies the effect of unbalanced diversity branches on the error probability performance. It can be noted that the system performs better if the branches with lowest severity parameters present the highest power.

B. M-PSK

We utilize the Moment Generator Function (MGF) technique to find an expression for the average probability of error for the M-PSK modulation in Nakagami-m fading. From (2.10),

$$P_s = \frac{1}{\pi} \int_0^{(M-1)\frac{\pi}{M}} \mu_{\gamma_{equ}}\left(-\frac{g}{\sin^2\phi}\right) d\phi \quad , \tag{2.20}$$

$$\mu_{\gamma_{equ}}\left(-\frac{g}{\sin^2\phi}\right) = \left(1 + \frac{g\,\gamma_{equ}}{m\,\sin^2\phi}\right)^{-m} \tag{2.21}$$

Following the same procedure mentioned above by taking m into consideration:

$$P_s = \frac{1}{\pi} \int_0^{(M-1)\frac{\pi}{M}} \prod_{i=1}^{k} \left(1 + \frac{g.\left(\gamma_{Tot}\left(\frac{k_i}{\sum_{i=1}^{k} k_i}\right)\right)}{m\sin^2\phi}\right)^{-mi} d\phi \quad . \tag{2.22}$$

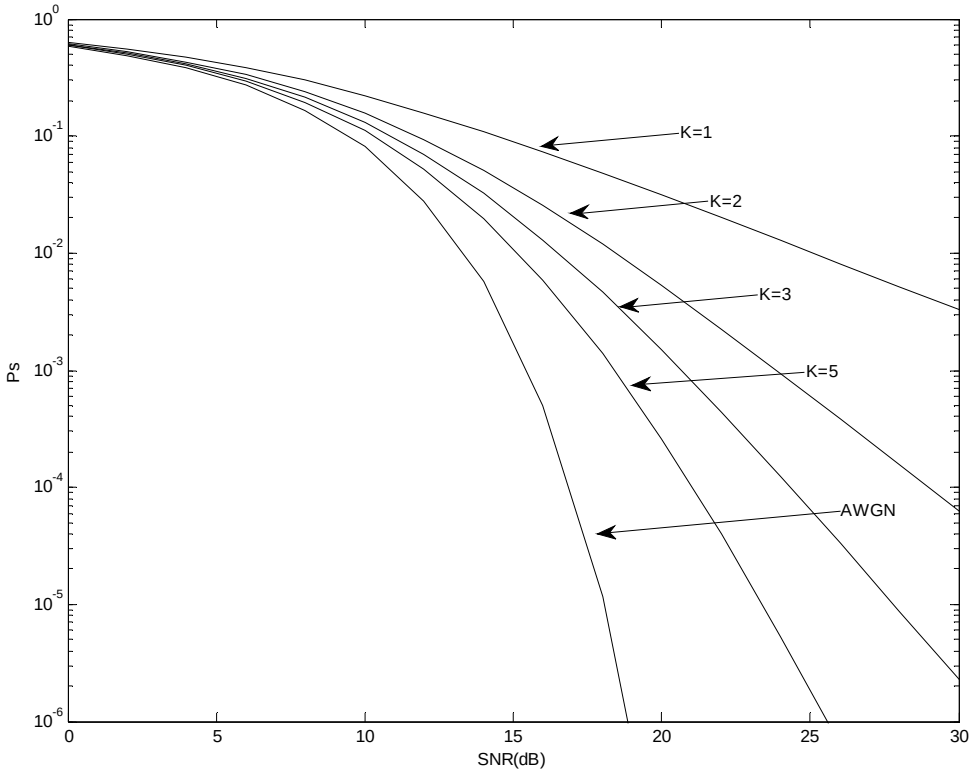

Fig. 12 Average symbol error probability versus average SNR per bit for 16-PSK signals with K=1, 2, 3, 5. (Rayleigh fading channels and AWGN).

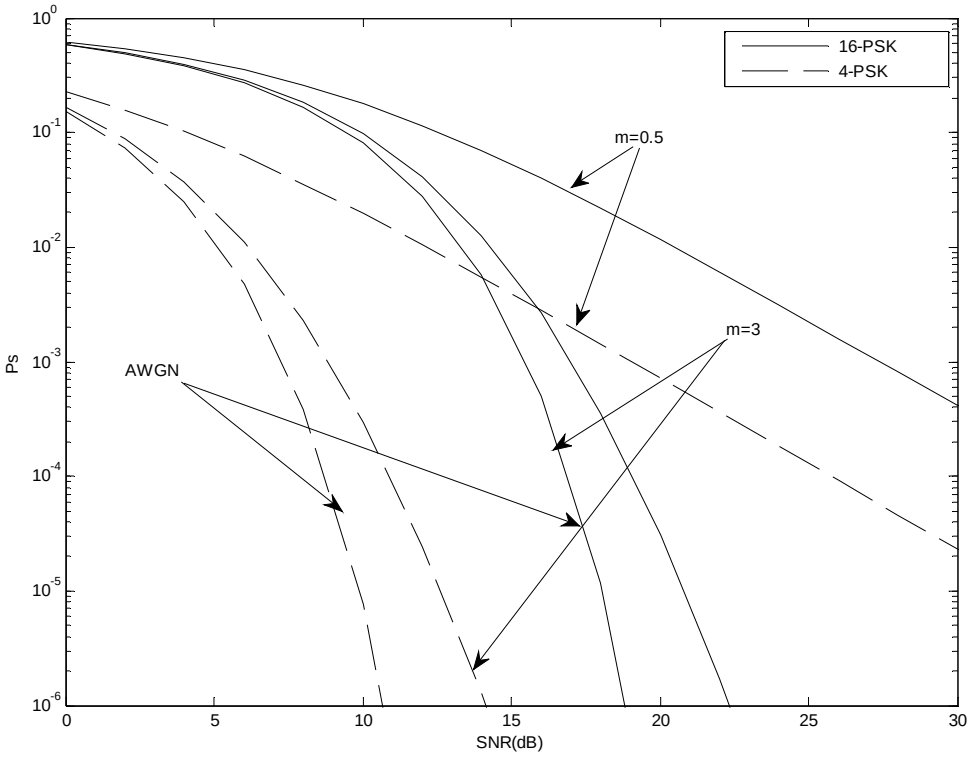

Fig. 13 Average symbol error probability versus average SNR per bit for (16- and 4-) PSK signals with k=1, Nakagami-m fading channel, and AWGN.

Fig. 13 illustrates the effect of the fading severity parameter on error probability performance and it can be seen that the system performs better under less severity (m increased).

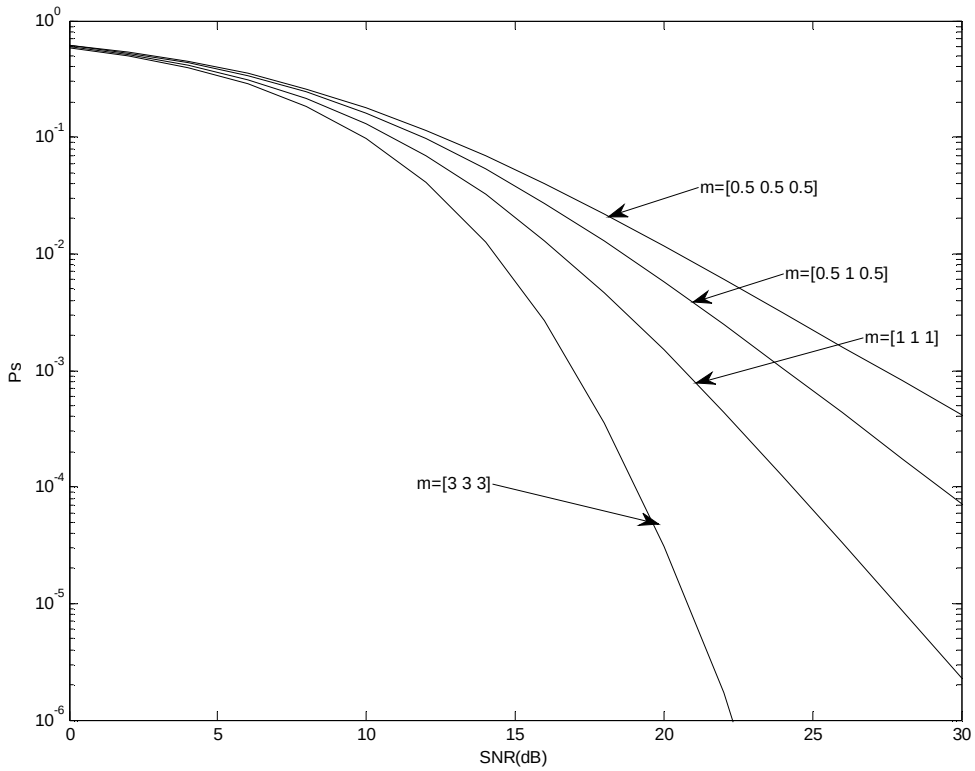

Fig. 14 Average symbol error probability versus average SNR per bit for 16-PSK signals with k=3, Nakagami-m fading channel with different fading-severity parameters.

The influence of the fading severity parameters is also studied in the Fig. 14 where three branches with different severity parameters are used. The branches with lowest severity parameters present the better performance.

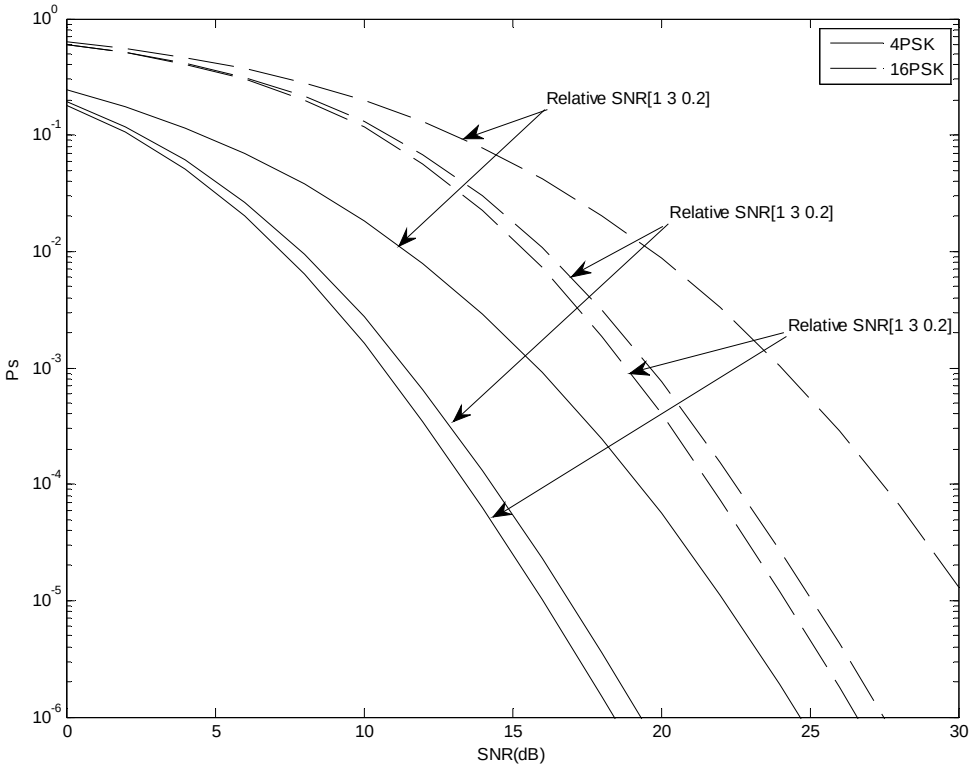

Fig. 15 Average symbol error probability versus average SNR per bit for (16- and 4-) PSK signals with 3 unbalanced diversity branches with m=1, 0.5,3 for k=1, 2, 3, respectively.

The effect of unbalanced diversity branches on the error probability performance is studied in Fig. 15. It can be noted that the system performs better if the branches with lowest severity parameters and the highest power.

2.3 K-M Parameter in Nakagami-m Fading Channel

The general expression for P_S of coherent modulation as defined in (2.11)

$$P_S = \int_0^{\infty} p_s(\gamma).p_{\gamma s}(\gamma)d\gamma \quad .$$

By using the alternative Q-function [12], the equation (2.11) can be written as

$$P_S = P_s(\gamma_s).\int_0^{\infty} p_\gamma(\gamma)d\gamma.\exp(-s\gamma) \ , \tag{2.23}$$

where α, g depend on the modulation, and s is a function of ϕ

Note that $\int_0^{\infty} p_\gamma(\gamma)d\gamma.\exp(-s\gamma)$ is the Laplace transform of the pdf of γ

and is defined as $\mu_s(s)$.

The MGF of Nakagami-m is given by [13]:

$$\mu_S(s) = \left(\frac{1}{1-\frac{s\gamma}{m}}\right)^m \ . \tag{2.24}$$

For m=∞, we obtain the form of type1^{∞}. The solution is given by introducing a dependant variable:

$$y = \left(\frac{1}{1-\frac{s\gamma}{m}}\right)^m \ . \tag{2.25}$$

and taking the natural logarithm of both sides:

$$\ln y = m \ln\left(\frac{1}{1 - s\gamma/m}\right) = \frac{\ln\left(\frac{1}{1 - s\gamma/m}\right)}{1/m}\ , \tag{2.26}$$

The limit

$$\lim_{m\to\infty} \ln y = \lim_{m\to\infty} \frac{\ln\left(\frac{1}{1 - s\gamma/m}\right)}{1/m} \tag{2.27}$$

is an indeterminate form of type 0/0, so by L'Hopital's rule,

$$\lim_{m\to\infty} \ln y = \lim_{m\to\infty} \frac{\ln\left(\frac{1}{1 - s\gamma/m}\right)}{1/m} = \lim_{m\to\infty} \frac{\left(\frac{-s\gamma}{m^2}\right) \Big/ (1 - s\gamma/m)}{-1/m^2} = \lim_{m\to\infty} \frac{s\gamma}{1 - s\gamma/m} = s\gamma, \tag{2.28}$$

Since $\ln y \to s\gamma$ as $m \to \infty$, it follows from the continuity of the natural exponential function that $e^{\ln y} \to e^{s\gamma}$ or equivalently, $y \to e^{s\gamma}$ as $m \to \infty$. Therefore,

$$\lim_{m\to\infty} \left(\frac{1}{1 - \frac{s\gamma}{m}}\right)^m = e^{s\gamma} \quad . \tag{2.29}$$

$\mu_\gamma(s) = \left(\frac{1}{1 - \frac{s\gamma}{mK}}\right)^{mK}$ which can be solved by following the same procedure as mentioned above.

In conclusion, when K= ∞, the channel converges to an AWGN channel.

3. AVERAGE SYMBOL ERROR PROBABILITY FOR DEPENDENT CHANNELS

3.1. Moment Generator Function (MGF) of Nakagami-m

To show the effects of the dependent case in our system, we just need to use the covariance matrix that shows how the *K* bands are dependent. Determining such a covariance matrix for dispersed spectrum cognitive radio systems require an extensive measurement campaign. In addition, since there is not such study in the literature, we use two correlation matrices in [14] for the sake of analysis, which are for linear and triangular arrays in space diversity. These two matrices are referred to as A and B configurations in this study

$$A = \begin{pmatrix} 1 & 0.795 & 0.605 \\ 0.795 & 1 & 0.795 \\ 0.605 & 0.795 & 1 \end{pmatrix} . \tag{3.1}$$

$$B = \begin{pmatrix} 1 & 0.727 & 0.913 \\ 0.727 & 1 & 0.913 \\ 0.913 & 0.913 & 1 \end{pmatrix} . \tag{3.2}$$

The MGF of dependent case is defined in [15] as

$$\mu(s) = \frac{1}{\prod_{n=1}^{N} \left(1 - 2S\lambda_n\right)^{\frac{1}{2}}} , \tag{3.3}$$

where $s = \frac{-g}{\sin(\phi)^2}$, $N = 2\sum_1^K m_k$. where λ_n stand for eigenvalues of covariance matrix Σ.

The covariance matrix $\sum$ of X is $E\left(\left(x-E(x)\right)-E\left(\left(x-E(x)\right)\right)^{T}\right)$ and is of dimensions $\left(2\sum_{l=1}^{k}m_l\right)\times\left(2\sum_{l=1}^{k}m_l\right)$ X has zero mean and coavarience matrix is defined as

$$\sum=\begin{bmatrix}\sigma_{11} & \sigma_{12} & \ldots & \sigma_{l,2m}\\ . & . & . & .\\ . & . & . & .\\ \sigma_{2,m_1} & \ldots & \ldots. & \sigma_{2m_i 2m_j}\end{bmatrix}, \tag{3.4}$$

where $\sigma_{n,k}=\left(\sqrt{\frac{\operatorname{cov}(\gamma_i,\gamma_j)}{4\min(m_i,m_j)}}\right)$. (3.5)

The dimension of covariance matrix depends on *N* which means that there are always $N-K$ repeated eigenvalues with $2m_i-1$ repeated eigenvalues per band. This is expected since the derivation depends on the facts that all the bands depend on each other. Thus (3.3) can be rewritten as

$$\mu(s)=\frac{1}{\prod_{i=1}^{k}\left(1-S(\gamma_i.e_i)\right)^{m_i}}. \tag{3.6}$$

3.2. Average Symbol Error Probability

The average symbol error probability for M-QAM is defined in (2.12) as:

$$=\frac{4}{\pi\log_2(M)}\left[\left(1-\frac{1}{\sqrt{M}}\right)\int_0^{\pi/2}\mu_{\gamma s}(s)d\phi-\left[\left(1-\frac{1}{\sqrt{M}}\right)^2\right]\int_0^{\pi/4}\mu_{\gamma s}(s)d\right], \tag{3.7}$$

where g is a function of the size of M-QAM, being defined as $g=\frac{1.5}{M-1}$.

The average symbol error probability for M-PSK modulation can be obtained, and the resultant expression is

$$\bar{P}_S = \frac{1}{\pi}\cdot \int_{o}^{(M-1)\frac{\pi}{M}} \left(\prod_{i=1}^{K} \left(1 - s(\gamma_i . e_i)\right)^{-m} \right) d\phi \quad . \tag{3.8}$$

3.3. Numerical Example

The covariance matrix of configuration A for three bands (k=3, m=1 Rayleigh) is given by (3.1):

$$A = \begin{pmatrix} 1 & 0.795 & 0.605 \\ 0.795 & 1 & 0.795 \\ 0.605 & 0.795 & 1 \end{pmatrix}$$

Step One: Find the dimension of matrix Σ. We use 3-bands and assume all of them are dependent, so the first step is to calculate the dimension of the covariance Σ that shows how the three bands depend on each other N=6, this represents the number of eigenvalues of matrix Σ, and its dimension.

Step Two: Finding the matrix Σ by taking the first element in (3.1) and substitute into (3.4). We obtain

$$\begin{bmatrix} 0.5 & 0 \\ o & 0.5 \end{bmatrix}$$

Then the covariance matrix Σ, for m=1, Rayleigh will be:

$$\Sigma = \begin{pmatrix} 0.5 & 0 & 0.446 & 0 & 0.389 & 0 \\ 0 & 0.5 & 0 & 0.446 & 0 & 0.389 \\ 0.446 & 0 & 0.5 & 0 & 0.446 & 0 \\ 0 & 0.446 & 0 & 0.5 & 0 & 0.446 \\ 0.389 & 0 & 0.446 & 0 & 0.5 & 0 \\ 0 & 0.389 & 0 & 0.446 & 0 & 0.5 \end{pmatrix} \tag{3.9}$$

Step Three: Find the eigenvalues of matrix Σ.

$$e = \begin{bmatrix} 0.0347 & 0.0347 & 0.1111 & 0.1111 & 1.3542 & 1.3542 \end{bmatrix}$$

In the same way, the eigenvalues of configuration B is

$e = [0.0047 \quad 0.0047 \quad 0.0737 \quad 0.0737 \quad 1.4216 \quad 1.4216]$

For m=0.5 (A) e= 0.049 0.1571 1.9152 and (B) e= 0.0066 0.1041 2.0106

For m=2.0 (A) e= 0.0245 0.0785 0.9576 and (B) e= 0.0033 0.0521 1.0052

Step Four: Find the equivalent SNR

The equivalent SNR can be expressed as: $\gamma_{Tot} = \gamma_1 + \sum_{i=2}^{K} \frac{\alpha_i}{\beta_i}\gamma = \gamma_1 + \sum_{i=2}^{K} k_i \gamma$, gamma is the

same for all branches, which means the $\gamma_{Tot} = 3\gamma$, and thus $\gamma = \frac{\gamma_{Tot}}{3}$. (3.10)

Step Five: Find MGF

Since we have 3 repeated eigenvalues, the MGF is going to be

$\frac{1}{\left(1 - s\left(e_1 \cdot \frac{\gamma_{equ}}{3}\right)\right)} \cdot \frac{1}{\left(1 - s\left(e_2 \cdot \frac{\gamma_{equ}}{3}\right)\right)} \cdot \frac{1}{\left(1 - s\left(e_3 \cdot \frac{\gamma_{equ}}{3}\right)\right)}$, then substitute into (3.6) and (3.7).

Note e_1, e_2, e_3 are 0.037, 0.1111, 1.3542, respectively.

Special Case:

If we have unbalance, RG= {1, 2, 0.5}. (3.11)

$\gamma_{equ} = \gamma + 2\gamma + 0.5\gamma = 3.5\gamma$. In this case $\gamma_1 = \frac{\gamma_{equ}}{3.5}, \gamma_2 = \frac{2\gamma_{equ}}{3.5}, \gamma_3 = \frac{\gamma_{equ}}{7}$ (3.12)

3.4 Numerical Results

Figures 16, 17 and 18 present the effect of fading correlation on the error probability performance of (4- and 16-) QAM signals, and 16-PSK for different values of m. The performances of the two covariance matrices A and B are studied. It can be seen that the correlation degrades the performance of the system and it can also be noted that A performs better than B and this is expected because it presents a lower correlation coefficients. Fig. 19 presents the performance comparison for the case of 16-QAM and

16-PSK modulation schemes. It is observed that the performance of 16-QAM is better than that of 16-PSK and this result can be justified since the distance between any points in the signal constellation of M-PSK is less than that in M-QAM.

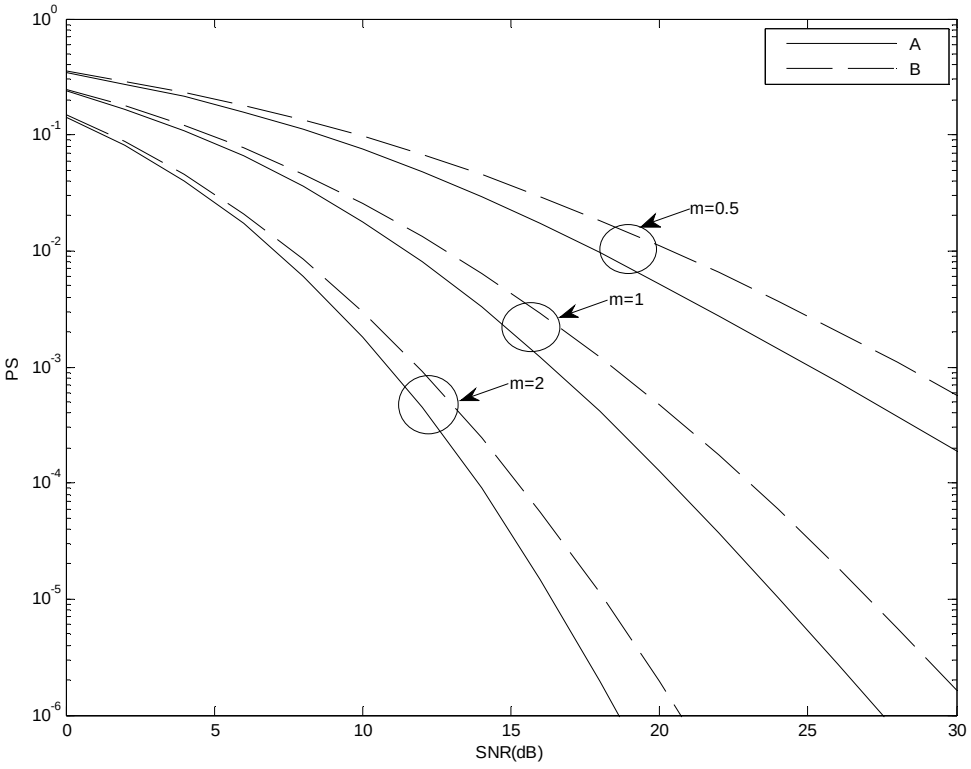

Fig. 16 Average symbol error probability versus average SNR per bit for 4-QAM signals with three correlated Nakagami fading channels for A and B configurations.

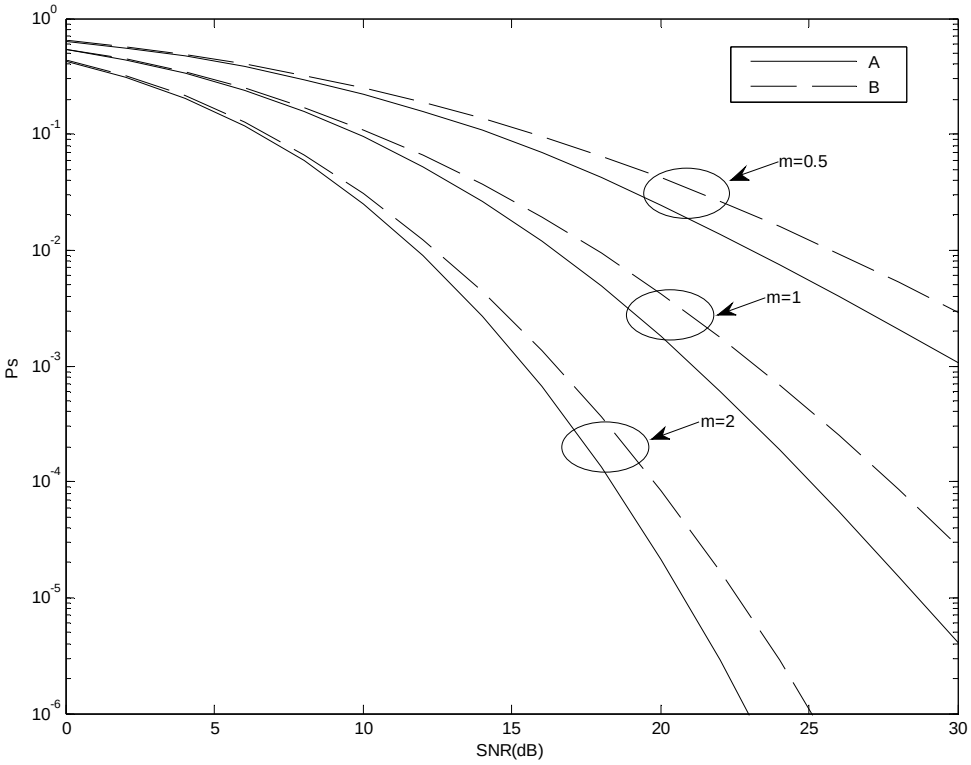

Fig. 17 Average symbol error probability versus average SNR per bit for 16-QAM signals with three dependent Nakagami fading channels for A and B configurations.

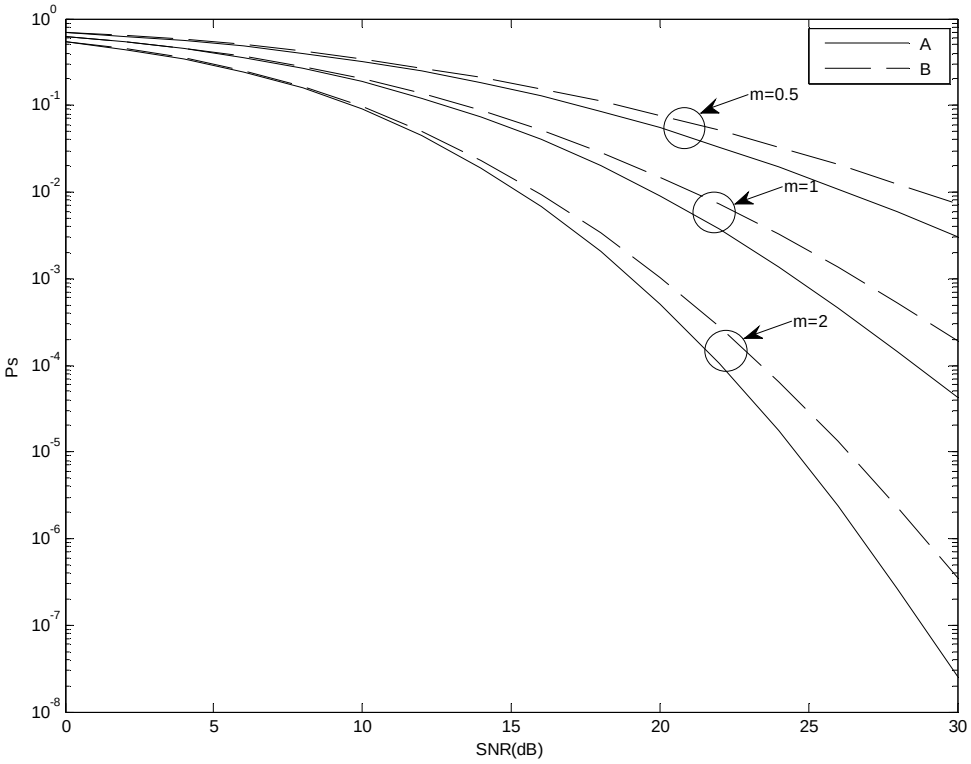

Fig. 18 Average symbol error probability versus average SNR per bit for 16-PSK signals with three dependent Nakagami fading channels for A and B configurations.

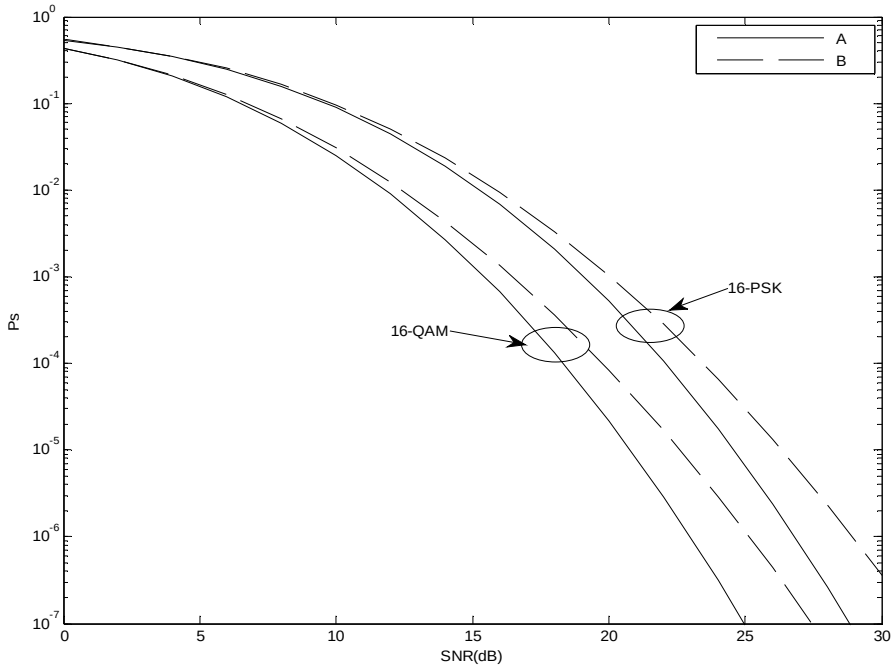

Fig. 19 Average symbol error probability versus average SNR per bit for 16-PSK, 16=QAM signals with three dependent Rayleigh fading channels for dependent and independent.

4. THE EFFECTS OF CODING ON DISPERSED SPECTRUM COGNITIVE RADIO SYSTEMS

4.1 Overview

In this section, the effect of coding on the performance of dispersed spectrum cognitive radio systems is investigated. Convolutional coding is different from block coding. The difference is that the convolutional coding consists of an encoder containing a memory which depends on the current input, and some previous inputs. The first idea of convolutional coding was introduced by Elias [16] as an alternative for block coding. The rate $R = \frac{k}{n}$ of convolutional encoder with memory m. Parameters k and n represent the input and the output, respectively. In [17], it was proposed an efficient decoding method for convolutional coding. However, the implementation is hard. In [18], it was proposed another method which is easy to implement with less efficient. Convolutional Coding has been presented in many books [19, 20, and 21]. In this section we will explain how convolutional encoder can be represented by using a state diagram and how the weight-enumerator function can be derived. The encoder in the convolutional coding can be classified into two categories: systematic and non-systematic, and it can be written as an (n,k,v) code, where v is the codeword [22].

If v_i is the length of the i^{th} shift register and input sequence k in a convolutional encoder, the encoder memory order can be defined as $m=\max[v_i]$ for $1 \le i \le k$, In our work, we used i=1.

4.2 Structural Properties of Convolutional Codes

There are some structural probabilities of convolutional codes that need to be considered [22]:

- The states are labeled as v-tuple: (s0, s1, …, s(2^v-1)). The number of states is 2^v states.
- The state diagram can be presented in a way to provide a complete description of the Hamming weights for all the nonzero code words.
- Weight numerating function (WEF) is obtained based on deleting self loop around s0, and Split s0 into initial and final.
- Label branches with branch gain X^i, where i is the weight of encoded bits on that branch.
- The WEF of a code can be determined by modifying state diagram to a signal flow graph for control theory.
- Applying Mason's gain formula [23]

  $A(x)=\text{sum}\ (A_i\ X^i)$, (4.1)

  where Ai is the number of code words of weight i.
- Loop with gain Ci is defined as a path starting at any state (except S0) and returning to that state through any other state twice.
- Forward path, Fi, is defined as a path starting at S0 initial and ending at S0 final.
- Non touching loops are defined as a set of loops called non touching loops meaning that no state can share more than one loop in the set.

(i) Set of all loops

(ii) (i', j') set of all pairs of non-touching loops.

(iii) (i", j", l") set of all triple non touching loops.

The codeword WEF of a code can be obtained by creating a modified state diagram of encoder as a signal flow graph and applying the Mason's gain formula[23].

$\Delta=1-\sum Ci + \sum Ci'Cj' - \sum Ci"Cj"Cl" + \ldots$, (4.2)

let $\Delta i=\Delta$ when states along ith forward path are removed

$WEF=\sum Fi\Delta i/\Delta = A(X)$. (4.3)

Additional information about the structure of the code can be obtained by using the code word IOWEF (input/output WEF)

$A(W,X,L)=\sum A_{j,i,l} W^j X^i L^l$, (4.4)

where $A_{j,i,l}$ stands for the number of code words of weight i with information weight j and length of the code l.

4.3 Encoding of Convolutional Coding

For a (2, 1, 3) code the generator matrices are: $g^{(0)}=(1\ 1\ 0\ 1)$, $g^{(1)}=(1\ 1\ 1\ 1)$

The number of states is $2^3 = 8$

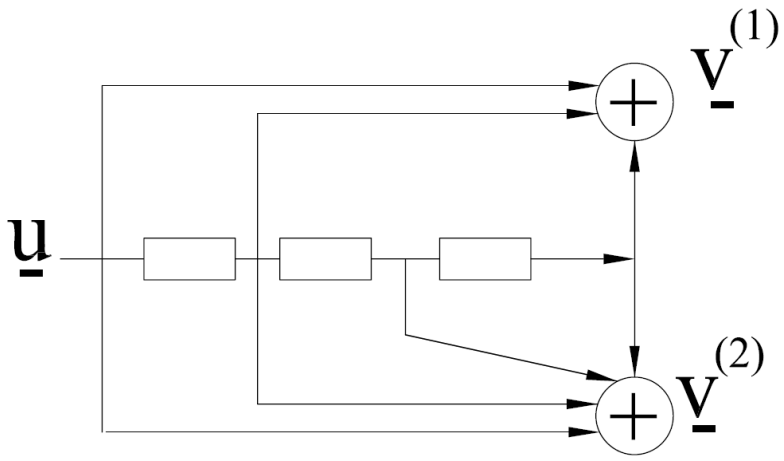

Fig. 20 A (2,1,3) systematic feedforword encoder.

From Fig, 20, we can write all possible states for this type of encoder. Table 1 shows all possible states for each new input.

Table.1 Shows the new states of encoder specified in the figure 20.

State	Input	Output	New State
S_0 0 0 0	0	0 0	0 0 0 S_0
S_0 0 0 0	1	1 1	1 0 0 S_4
S_1 0 0 1	0	1 1	0 0 0 S_0
S_1 0 0 1	1	0 0	1 0 0 S_4
$S2$ 0 1 0	0	0 1	0 0 1 S_1
$S2$ 0 1 0	1	1 0	1 0 1 S_5
S_3 0 1 1	0	1 0	0 0 1 S_1
S_3 0 1 1	1	0 1	1 0 1 S_5
S_4 1 0 0	0	1 1	0 1 0 $S2$
S_4 1 0 0	1	0 0	1 1 0 S_6
S_6 1 01	0	1 0	0 1 1 S_3
S_6 1 1 0	1	0 1	1 1 1 S_7
S_7 1 1 1	0	0 1	0 1 1 S_3
S_7 1 1 1	1	1 0	1 1 1 S_7

We can rewritten the states above as diagram as shown in Fig 21

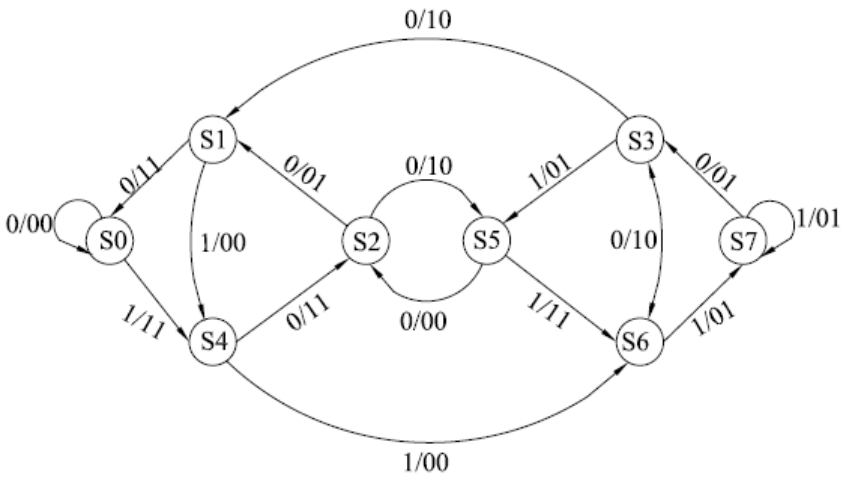

Fig 21 Encoder state diagrams for (2, 1, 1) encoder of figure 20.

According to the state diagram we can find the loops.

Table 3 Loops generated by figure 21.

$S_1\ S_7$	$S_4\ S_6\ S_3\ S_5\ S2\ S_1\ S_4$
$S_3\ S_5\ S_6\ S_3$	$S_4\ S_6\ S_7\ S_3\ S_1\ S_4$
$S_4\ S_1\ S2\ S_4$	$S_4\ S_6\ S_7\ S_3\ S_1\ S_4$
$S2\ S5\ S2$	$S_4\ S2\ S_5\ S_6\ S_3\ S_4$
$S_4\ S_6\ S_3\ S_1\ S_4$	$S_4\ S_6\ S_7\ S_3\ S_5\ S2\ S_1\ S_4$

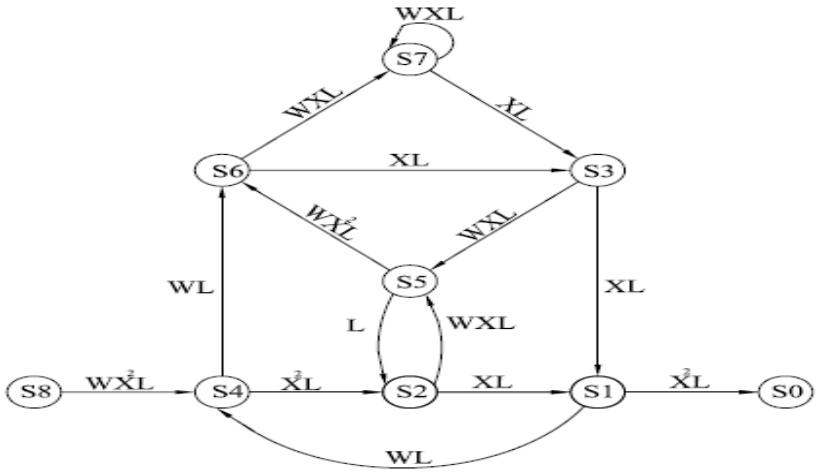

Fig. 22 Modified encoder state diagrams for (2,1,3) of encoder of figure 21.

C_1=XWL

$C_2 = W^2X^4L^3$

$C_3 = WX^3L^3$

$C_4 = W\ \ XL^2$

$C_5 = W^2X^2L^4$

$C_6 = W^3X^3L^6$

$C_7 = W^3X^3L^5$

$C_8 = W^3X^7L^6$

$C_9 = W^4X^4L^7$

$C_{10} = W^4X^8L^7$

$C_{11} = W^3X^5L^4$

Triple non-touching Loops:

$T_1 = C_1C_4C_5 = W^4X^4L^7$

$T_2 = C_1C_2C_3 = W^4X^8L^7$

Pairs of non-touching loops

$P_1 = C_1C_2 = W^3X^5L^4$

$P_2 = C_1C_3 = W^2X^4L^4$

$P_5 = C_1C_6 = W^4X^4L^7$

$P_6 = C_1C_8 = W^4X^8L^7$

$$P_3 = C_1 C_4 = W^2 X^2 L^3 \qquad P_7 = C_4 C_5 = W^3 X^3 L^6$$

$$P_4 = C_1 C_5 = W^3 X^3 L^5 \qquad P_8 = C_4 C_7 = W^4 X^4 L^7$$

$$\Delta = 1 - \sum C_i + C_i^{/} C_j^{/} - \sum C_i^{//} C_j^{//} C_l^{//}, \tag{4.5}$$

$$= 1 - XW\left[L + L^2\right] - X^2 W^2 \left[L^4 - L^3\right] - W^2 X^4 \left[L^3 - L^4\right] - WX^3 L^3. \tag{4.6}$$

Forward Paths

$$F_1 = W^2 X^7 L^4 \qquad F_5 = W^4 X^8 L^8$$

$$F_2 = W^2 X^6 L^5 \qquad F_6 = W^3 X^{11} L^7$$

$$F_3 = W^7 X^7 L^6 \qquad F_7 = W^4 X^{12} L^8$$

$$F_4 = W^3 X^7 L^7$$

$$\Delta_1 = 1 - XWL - W^2 X^4 L^3 \qquad \Delta_3 = 1 - XWL^2$$

$$\Delta_2 = 1 - XWL\left[1 + L\right] - W^2 X^2 L^3 \qquad \Delta_4 = 1 - XWL$$

$$\Delta_5 = 1 \qquad \Delta_6 = 1 - XWL$$

$$\sum F_i \Delta_i = WX^7 L^4 - W^2 X^8 L^5 + W^2 X^6 L^5 \tag{4.7}$$

$$A(x, w, l) = \frac{WX^7 L^4 + W^2 X^6 L^5 - W^2 X^8 L^5}{1 - XW\left[L + L^2\right] - X^2 W^2 \left[L^4 L^3\right] - X^3 WL^3 - X^4 X^2 \left[L^3 - L^4\right]} \tag{4.8}$$

4.4 Average Symbol Error Probability Bound

We use the numerical results we obtained in previous work to apply the concept of convolutional coding in dispersed spectrum cognitive radio systems. The error probability is defined in [22] and bounded by

$$P_b(E) < \sum_{d=d_{free}}^{\infty} B_b p_d < B(x)\Big|_{x=2\sqrt{p(1-p)}} = \frac{1}{k}\partial \frac{A(w,x)}{\partial w}\Big|_{w=1} \quad , \tag{4.9}$$

where B_d is the number of non-zero information bits on all weight d-Paths.

Pd; and $A'(W,X) = \dfrac{WX^7 + W^2\left(X^6 - X^8\right)}{1 - W\left(2X + X^3\right)^2}$. (4,10)

$$\partial \frac{A(w,x)}{\partial w}\Big|_{w=1} = \frac{2X^6 - X^7 - 2X^8 + X^9 + X^{11}}{(1 - 2X - X^3)^2} \quad . \tag{4.11}$$

4.5 Numerical Results

The effect of coding on the performance of the system is investigated. The convolutional coding with the (2,1,3) code and $g^{(0)}$=(1 1 0 1), $g^{(1)}$=(1 1 1 1) generator matrices are considered. The bound for error probability in (4.9) is extended for our system and it is used as performance metric during the simulations. Finally, Nakagami-m fading channel along with M-PSK and M-QAM modulations are assumed. The results are plotted in Figs. 23 and 24, which show the effects of coding on the performance and it can be clearly seen that the performance is improved due to the coding gain.

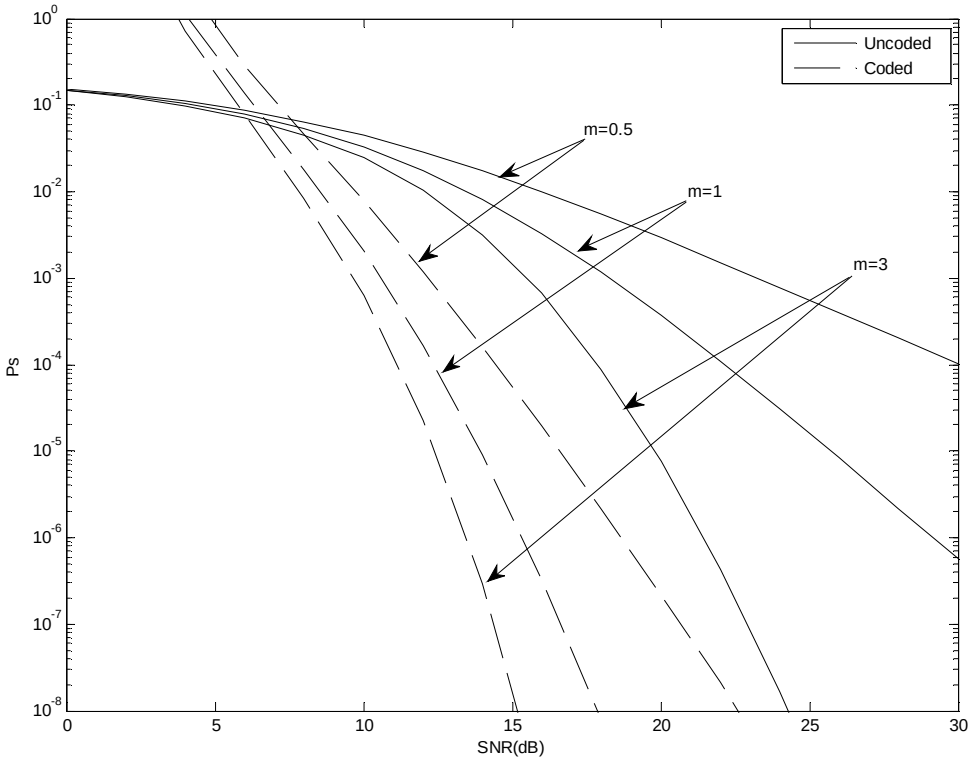

Fig. 23 Average bit error probability versus average SNR per bit for 16-PSK signals with k=1, Nakagami-m fading channel compared with the performance bound for convolutional codes.

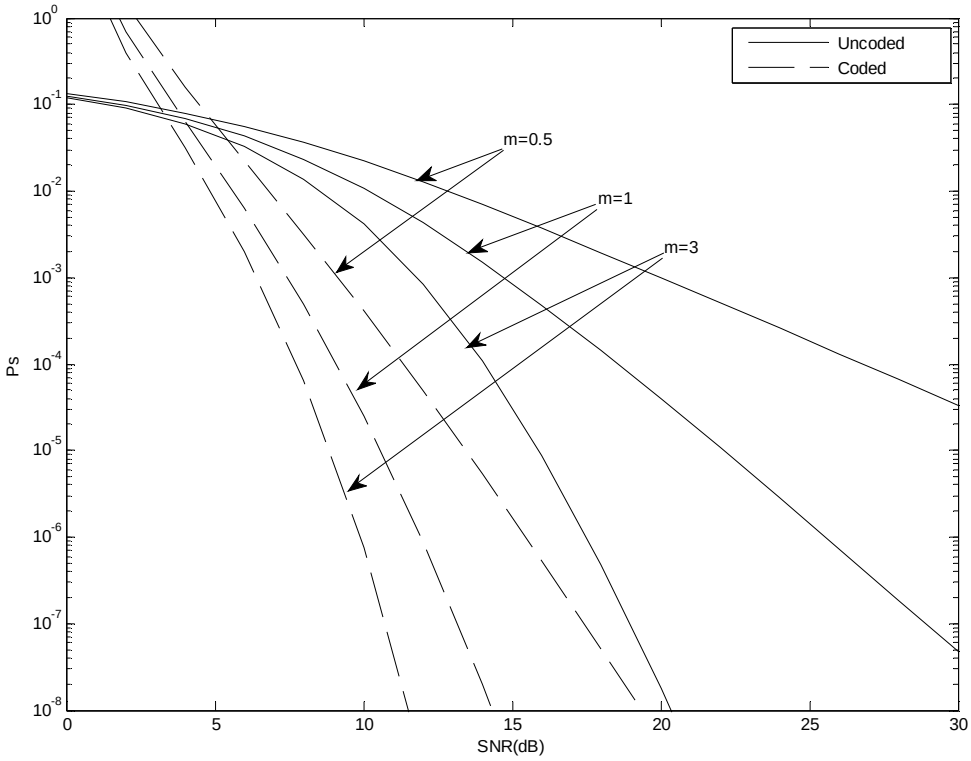

Fig. 24 Average bit error probability versus average SNR per bit for 16-QAM signals with k=1, Nakagami-m fading channel compared with the performance bound for convolutional codes.

5. PERFORMANCE ANALYSIS OFAD HOC DISPERSED SPECTRUM COGNITIVE RADIO SYSTEMS

5.1 Overview

Wireless ad hoc networks have become an important area of research in wireless communications systems due to their advantage that they can be deployed without requiring any preexisting infrastructure. Ad hoc networks neither have fixed topology nor centralized servers; once an ad hoc network is deployed, the network nodes would be self-controlled to form a communication network and provide connectivity to the destination to deliver the data throughout hops with an acceptable bit error rate [4, 5].

In [24], 2-D and 3-D structures for underwater sensor networks are proposed where the main objective was to determine the minimum numbers of sensors and redundant sensor nodes for achieving communication coverage. In [25], the effect of non-uniform random node distributions on the throughput of MAC protocol is investigated through simulation without providing theoretical analysis. In [26], 3-D configuration based method that provides smaller number of path and better energy efficiency is proposed. Furthermore, several studies in the literature have studied the use of location information in order to enhance the performance of cognitive radio networks [27, 28]. It is concluded that use of network topology information could bring significant benefits to cognitive radios and networks to minimize the maximum transmission power and reduce the spectral impact of the topology [29].

The previous works motivate us to investigate the effects of 3-D node distribution on the effective transport capacity of ad hoc dispersed spectrum cognitive radio systems. Note that the effective transport capacity concept has been introduced in [6], which

quantifies the maximum bandwidth-distance product that can be supported by the network. In this section, the evaluation of the effective transport capacity of ad hoc dispersed spectrum cognitive radio systems considering 3-D configuration is carried out realistic cases. We considered the following two MAC protocols for the INI case:

- Reserve-and-go (RESGO): A node reserves a route to destination and transmits the information without looking at the status of the channel.
- Reserve-*listen* and- go (RESLIGO): A node reserves a route to a destination and looks at the status of channel before sending the information over the route.

The most important parameter in wireless communications is the bit error rate (BER). The derivation of BER for dispersed spectrum cognitive radio systems is based on the fact that the summation of error probability and probability that there is no error is one and since all hops are independent, the average BER of dispersed spectrum cognitive radio systems for a given source destination path can be expressed as

$$\mathrm{BER}^{(n)} \approx 1 - (1 - \mathrm{BER}_L)^n \qquad (5.1)$$

where BER_L is BER at the end of a single link, and n stands for the number of hops.

To find out an average network performance of ad hoc dispersed spectrum cognitive radio systems, it is considered a route with an average number of hops $\bar{n}_h$. To do so, it is required to identify the maximum number of hops $n_h^{\max}$ and a probability distribution for the number of hops n_h, which is an integer between 1 and $n_h^{\max}$. We could find a route having a minimum of nodes which represents a straight line by assuming that the source and destination nodes lie at the opposite ends of a diameter over a spherical surface and a large number of nodes in the network are simulated. The maximum number of hops $n_h^{\max}$ can be expressed as [7]:

$$n_h^{\max} = \left\lfloor \frac{diameter_{surface}}{d_{link}} \right\rceil \quad , \tag{5.2}$$

where $\lfloor \ \rceil$ indicates the integer value closest to the argument.

The number of hops is considered to be any symmetric probability distribution which means that the average number of hops $\overline{n_h} = n_h^{\max} / 2$. This is the case, for example, of a PDF for n_h given by considering a uniform distribution as follows

$$P_{n_h}(x) = \begin{cases} \frac{1}{n_h^{\max}}, & 0 < x < n_h^{\max} \\ 0, & otherwise \end{cases} \quad , \tag{5.3}$$

And then

$$\overline{n}_h = \int_0^{n_h^{\max}} \frac{1}{n_h^{\max}} x dx = \frac{n_h^{\max}}{2} \tag{5.4}$$

The network communication system model can be summarized by the following points [6-8]:

- Each node transmits a fixed power and the multi-hop routes between a source and destination is established by a sequence of minimum length links.
- If a node needs to communicate with another node, a multi hop route is first reserved and only then can the packets be transmitted without looking at the status of the channel which is based on MAC protocol for INI: Reserve and Go (RESGO). Packet generation at each node is given by a Poisson process with parameter $\lambda_l \leq R_b$ (packets/second). Each packet has a fixed length of L bits.
- A necessary condition that needs to be satisfied for network communications is $\lambda \ L \leq R_b$, where R_B the transmission data rate of the nodes is.

The effective transport capacity is defined in [7] as

$$C_{T,e} = \lambda L \bar{n}_{sh} d_l N_{ar} \ , \tag{5.5}$$

where N_{ar} is the number of disjoint routs and $\bar{n}_{sh}$ is the average number of sustainable hops [5-8] which is defined as

$$\bar{n}_{sh} = \min\left\{n_{sh}^{\max}, \bar{n}_h\right\} = \min\left\{\left\lfloor \frac{\ln\left(1 - BER^{\max}\right)}{\ln\left(1 - BER_L\right)} \right\rfloor, \bar{n}_h\right\} \ , \tag{5.6}$$

where r_L is the distance that the data across the route with acceptable bit error rate.

It is known that the BER depends on the SNR. Donating the SNR at the end of a single link by SNR_L and assuming that the nodes interfere with each other, the SNR_L can be expressed as [7]

$$SNR_L = \alpha^2 \frac{\mu P_t / d_l^2}{FKT_0 R_b + P_{INT}\eta} \ , \tag{5.7}$$

where P_t, $K = 1.38 \times 10^{-23} J/K$, F , α, $T = 300K$, η , and P_{INT}, are the transmitted power from each node, the Boltzmann's constant, the noise figure, , the fading envelope, the room temperature, the spectral efficiency, the inter-node interference power which is defined as

$$\mu = \frac{G_t G_r c^2}{(4\pi)^2 f_l f_c^2} \ , \tag{5.8}$$

where G_t, G_r, c, f_c, and $f_l \le 1$ are the transmitter gain, receiver gain, the speed of light, the carrier frequency, a loss factor, respectively.

5.2. Two Dimensional Configuration

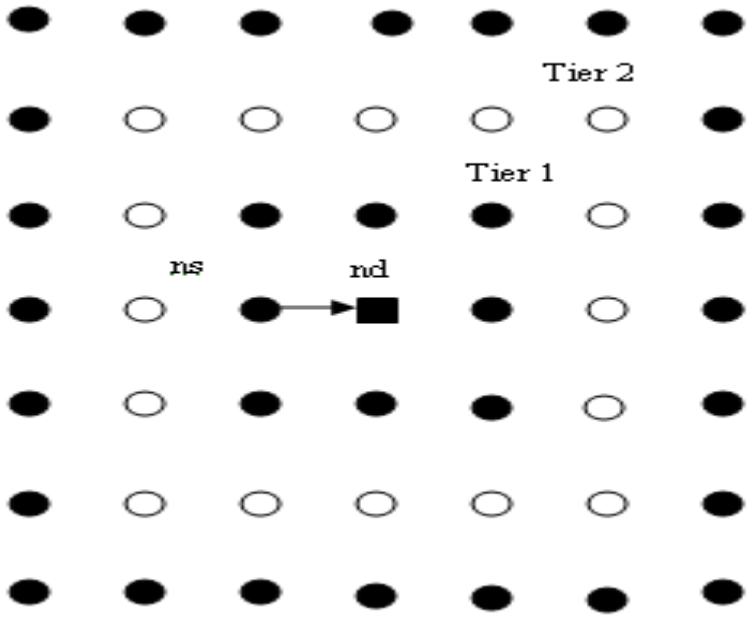

Fig. 25 Structure for 2-D distribution of an ad hoc wireless network [7].

In the i^{th} order tier of the 2-D distribution there are [7]:

- Four nodes at distance $i\ d_l$. The interference power at the destination node from any of these nodes is $\mu P_t / (d_l i)^2$.
- Eight nodes at distance $\sqrt{i^2 + j^2}\, d_l$, $j=1,\ldots,i-1, i \geq 2$ (i.e. a total of $8(i\text{-}1)$ nodes). The interference power at the destination node from any of these nodes is $\mu P_t / d_l^2 (i^2 + j^2)$.

- Four nodes at distance $i\sqrt{2}d_l$. The interference power at the destination node from any of these nodes is $\mu P_t / 2(d_l i)^2$.

Since the number of nodes in the network is finite, the maximum tier order $i^{\max}$ depends on the number of nodes *N* in the network which can be expressed for 2-D distribution as

$$N \approx \sum_{i=1}^{i_{\max}} 8i = 4i_{\max}\left(i_{\max} + 1\right) \ . \tag{5.9}$$

and

$$P_{INT}^{RESGO} \approx \mu P_t \rho_s \left(1 - e^{-\frac{\lambda L}{R_b}}\right) \Delta_A(N) \ , \tag{5.10}$$

where

$$\Delta_A(N) = \sum_{i=1}^{\lfloor \sqrt{N}/2 \rfloor} \left(\frac{6}{i^2} + 8 \sum_{j=1}^{i-1} \frac{1}{i^2 + j^2} \right) - 1 \ . \tag{5.11}$$

5.3 Three Dimensional Configuration

The node distribution, defined as 3D distribution, is that N nodes each are placed uniformly, at the centers of a cubic grid, in a Spherical volume V as in Fig. 26. Since $V \approx N d_l^3$, it can be easily shown that two neighboring nodes are at distance

$$d_l \approx (1/\rho_s)^{\frac{1}{3}} \ , \tag{5.12}$$

where $\rho_s = N/V$ (unit m^{-3}) is the node volume density.

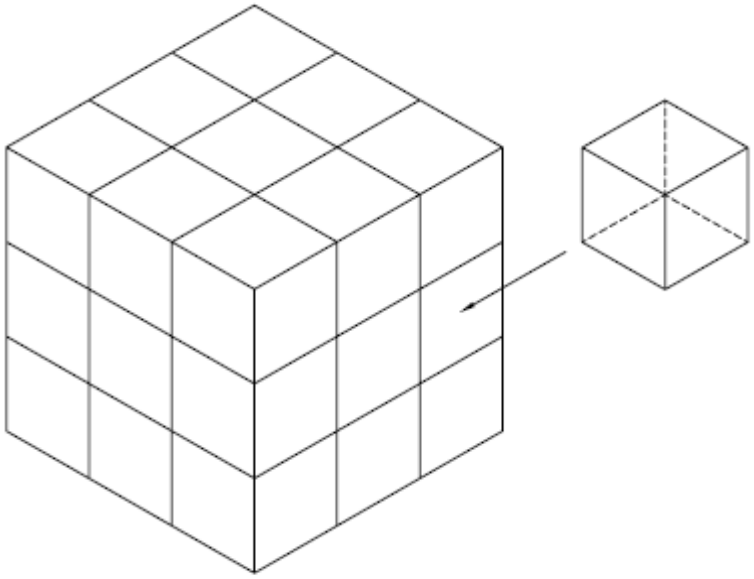

Fig. 26 Structure for 3-D distribution of an ad hoc wireless network.

1. Average Number of Hops

The first step is to calculate the average number of hops in the Ad hoc network. To do so, we will need to find the maximum number of hops and then find the average number of hops

n_h since the node distribution is uniform. By Assuming that the source and destination nodes lie at opposite ends of a diameter over a spherical surface, and a large number of nodes in the network are simulated which $n_h^{\max}$ for 3D distribution can be expressed as in (5.3)

$$n_h^{\max} = \left\lfloor \frac{diameter}{d_l} \right\rfloor = \left\lfloor \frac{2\left(\frac{3V}{4\pi}\right)^{1/3}}{\left(\frac{V}{N}\right)^{1/3}} \right\rfloor = \left\lfloor 2\left(\frac{3N}{4\pi}\right)^{1/3} \right\rfloor \quad , \tag{5.13}$$

It can be immediately concluded from (5.5) that

$$\overline{n_h} = n_h^{\max} / 2 , \tag{5.14}$$

$$\overline{n_h} = \left\lfloor \left(\frac{3N}{4\pi} \right)^{1/3} \right\rfloor , \tag{5.15}$$

2. Inter-node Interference (INI)

In the i^{th} order tier of the 3D distribution there are:

- 6 nodes at distance $i.d_l$, which represents the order of the tier, and d_l is the length of the edge of a cube. The interference power at the destination node from any of these nodes is $\mu P_t / (d_l i)^2$
- 8 nodes at distance $i\sqrt{3}d_l$. The interference power at the destination node from any of these nodes is $\mu P_t / 3(d_l i)^2$.
- 12 nodes at distance $i\sqrt{2}d_l$. The interference power at the destination node from any of these nodes is $\mu P_t / 2(d_l i)^2$.
- 24 nodes at distance $\sqrt{i^2 + j^2}d_L$, j=1,…,i-1, $i \geq 2$,. The interference power at the destination node from any of these nodes is $\mu P_t / d_l^2 (i^2 + j^2)$.
- 24 nodes at distance $\sqrt{2i^2 + j^2}d_L$, j=1,…,i-1, $i \geq 2$. The interference power at the destination node from any of these nodes is $\mu P_t / d_l^2 (2i^2 + j^2)$.
- 24 nodes at distance $\sqrt{i^2 + j^2 + z^3}d_L$, j=1,…,i-1, z=1,…,i-1, $i \geq 2$. The interference power at the destination node from any of these nodes is $\mu P_t / d_l^2 (i^2 + j^2 + z^3)$.

Since the number of nodes in the network is finite, there exists a maximum N.

$$N \approx \sum_{i=1}^{i_{\max}} (2i+1)^3 - (2(i-1)+1)^3 , \tag{5.16}$$

$$\sum_{i=1}^{i_{\max}} 24i^2 + 2 = 24\frac{i_{\max}(i_{\max}+1)(2i_{\max}+1)}{6} + 2i_{\max} , \tag{5.17}$$

Form (5.17), it leads to $i_{\max} \approx \lfloor (N)^{1/3}/2 \rfloor$.

In [7], the probability of a single bit in the packet interfered by any node in the network is defined as (1-exp (-λL/Rb)) which means that the overall interference power for 3-D configuration can be expressed as:

$$P_{INT}^{RESGO} = \mu P_t \rho_s^{2/3} \left(1 - e^{-\frac{\lambda L}{R}}\right) \times (\Delta_1 + \Delta_2 + \Delta_3 - 1), \tag{5.18}$$

where

$$\Delta_1 = \sum_{i=1}^{\frac{N^{1/3}}{2}} \frac{44}{3i^2} , \tag{5.19}$$

$$\Delta_2 = \sum_{i=2}^{\frac{N^{1/3}}{2}} \sum_{j=1}^{i-1} \left(\frac{24}{2i^2 + j^2} + \frac{24}{i^2 + j^2} \right) , \tag{5.20}$$

$$\Delta_3 = \sum_{i=2}^{\frac{N^{1/3}}{2}} \sum_{j=1}^{i-1} \sum_{z=1}^{i-1} \frac{24}{i^2 + j^2 + z^2} , \tag{5.21}$$

5.4 Summary

Finally, we summarize all parameters of the network for both node distributions in Table 3.

Table 3: Comparison for all network parameters between two and three dimensional distribution.

Preliminaries	Node Distribution	
	Two dimensional	Three dimensional
dl	$1/\sqrt{\rho_S}$	$d_l \approx (1/\rho_s)^{\frac{1}{3}}$
$\overline{n}_h$	$\lfloor \sqrt{N/\pi} \rfloor$	$\left\lfloor \left(\frac{3N}{4\pi}\right)^{1/3} \right\rfloor$
Nar	$\sqrt{N\pi}$	$N^{2/3}\left(\frac{4\pi}{3}\right)^{1/3}$
P_{int}	$P_{INT} \approx \mu P_t \rho_s \left(1 - e^{-\frac{\lambda L}{R_b}}\right) \Delta_A (N$ $\Delta_A(N) = \sum_{i=1}^{\lfloor \sqrt{N}/2 \rfloor} \left(\frac{6}{i^2} + 8\sum_{j=1}^{i-1} \frac{1}{i^2 + j^2}\right) - 1$	$P_{INT}^{RESGO} = \mu P_t \rho_s^{2/3} \left(1 - e^{-\frac{\lambda L}{R}}\right) \times (\Delta_1 + \Delta_2$ $\Delta_1 = \sum_{i=1}^{\frac{N^{1/3}}{2}} \frac{44}{3i^2}$ $\Delta_2 = \sum_{i=2}^{\frac{N^{1/3}}{2}} \sum_{j=1}^{i-1} \left(\frac{24}{2i^2 + j^2} + \frac{24}{i^2 + j^2}\right)$ $\Delta_3 = \sum_{i=2}^{\frac{N^{1/3}}{2}} \sum_{j=1}^{i-1} \sum_{z=1}^{i-1} \frac{24}{i^2 + j^2 + z^2}$ $\Delta_A^{odd}(N) =$ $\sum_{\substack{i=1 \\ i(odd)}}^{\lfloor \sqrt{N/3} \rfloor} \sum_{j=0}^{\frac{i-1}{2}} \left(\frac{12}{i^2 - (i/2)^2 + (0.5 + j)^2}\right) - \frac{6}{i^2}$

5.5 Numerical Results

We studied just one type of channel, 3-Rayleigh channels (Nakagami-m, m=1) for QAM, and M-PSK in both cases, independent, and dependent case. They are two types of correlations, namely linear and triangular defined in [14]. The triangular configuration has a large covariance coefficient larger than that in linear configuration.

Figs. 25 and 26 representing the new distribution system (3D), clearly show that the effective transport capacity (CT) is improved when using the 3D configuration. In Figs, 27, 28, 29, and 30 show 2D configuration. We also note that the independent case is the best one in all figures which is an expected result.

We have assumed that the gain of the transmitter and receiver is 1, loss factor is 1.56dB, noise figure is 6 dB, the carrier frequency is 2.4 GHz, and the network volume is $V = 1 \times 10^6 m^3$.

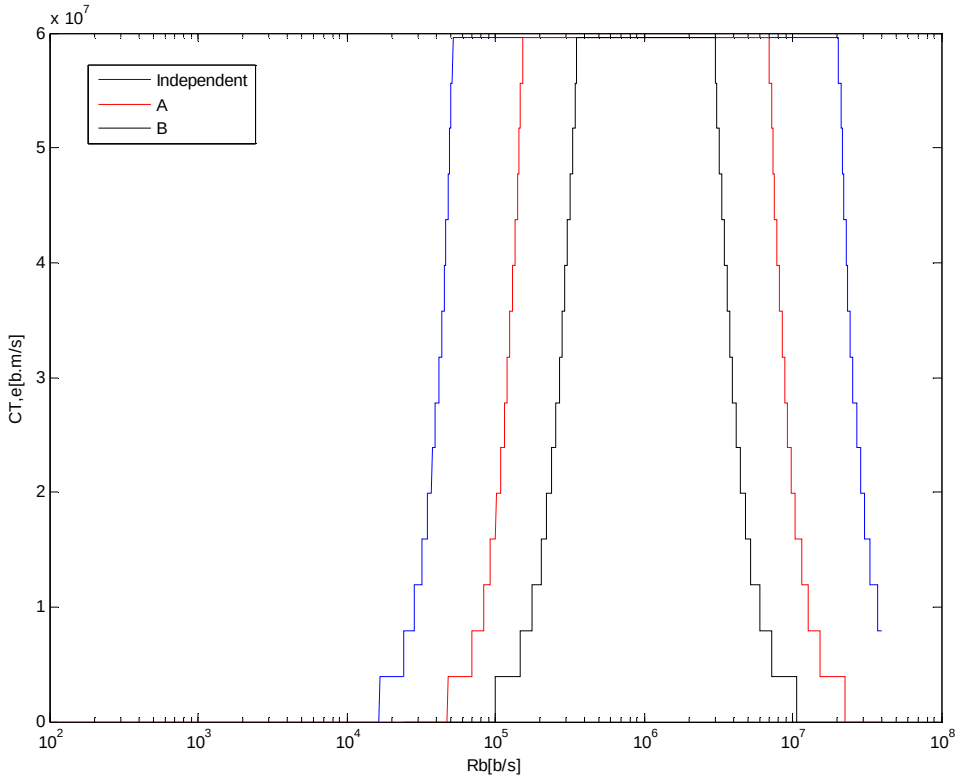

Fig. 27 3-D Effective Transport Capacity versus Rb for 4-QAM modulation with 3 Rayleigh fading channels.

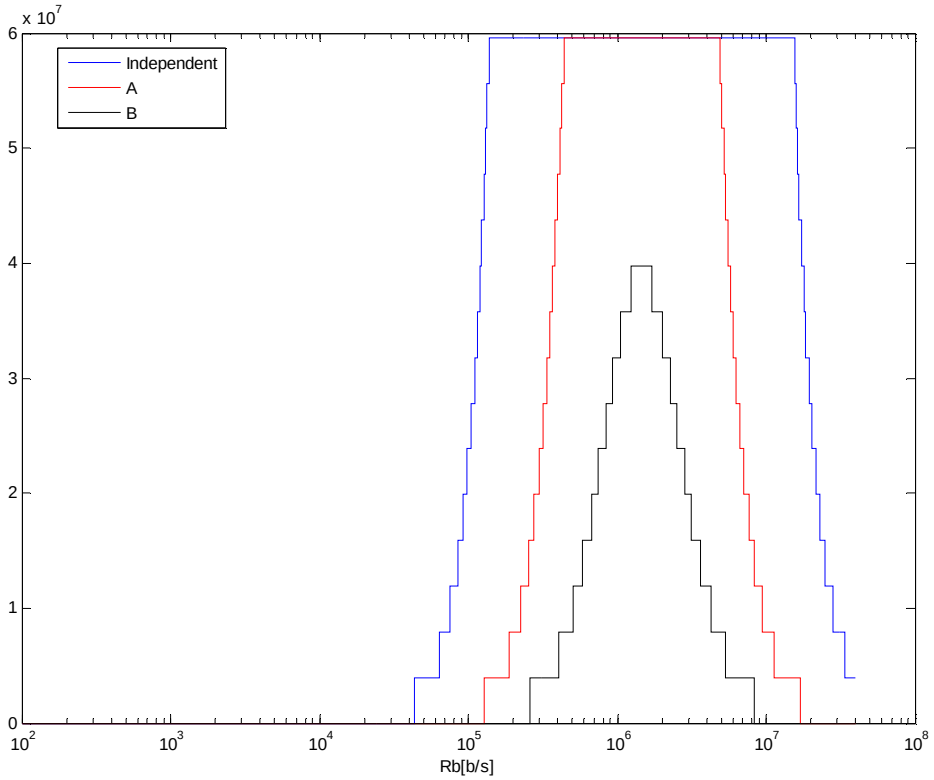

Fig. 28 3-D Effective Transport Capacity versus Rb for 16-QAM modulation with 3 Rayleigh fading channels.

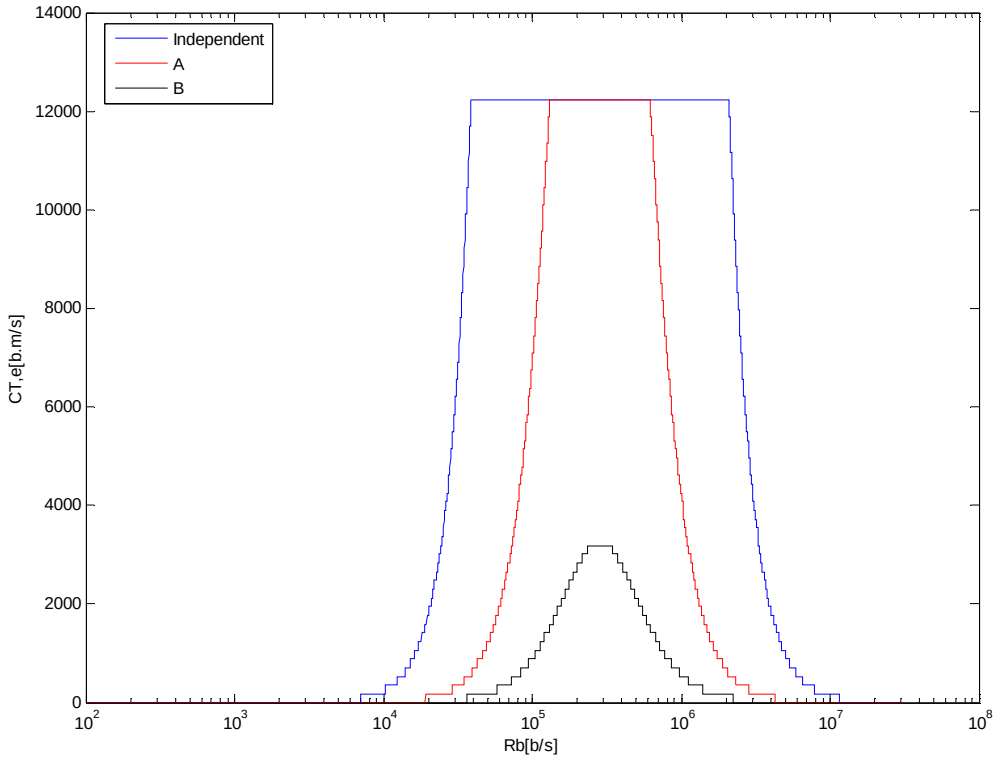

Fig. 29 2-D Effective Transport Capacity versus Rb for 16-PSK modulation with 3 Rayleigh fading channels.

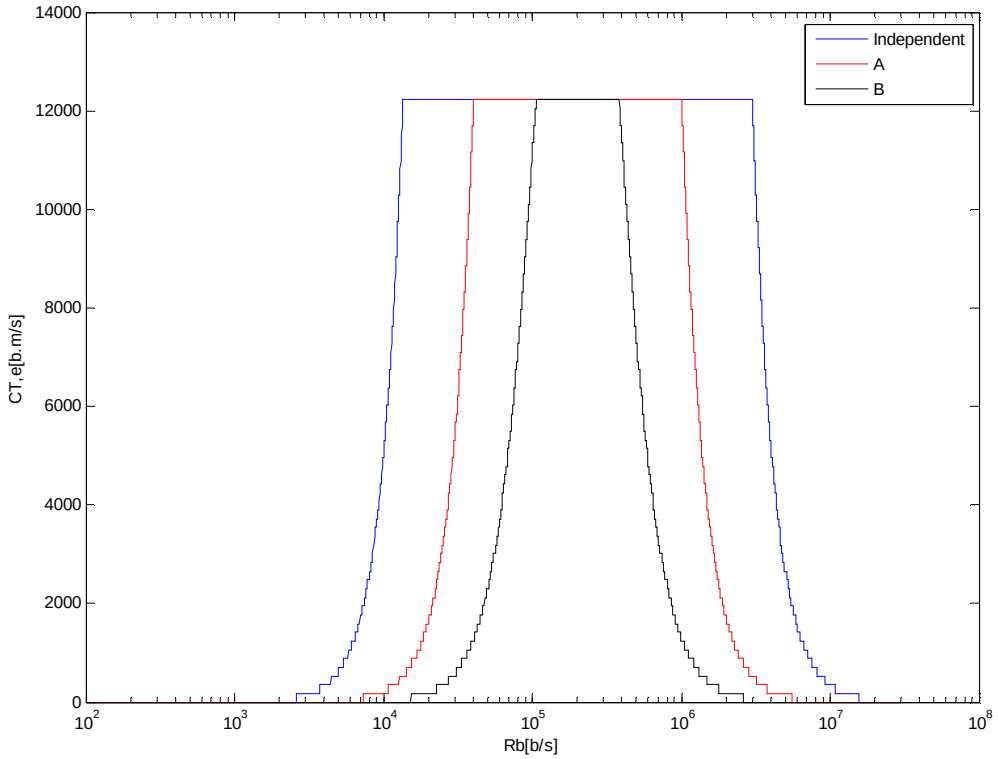

Fig. 30 2-D Effective Transport Capacity versus Rb for 4-QAM modulation with 3 Rayleigh fading channels.

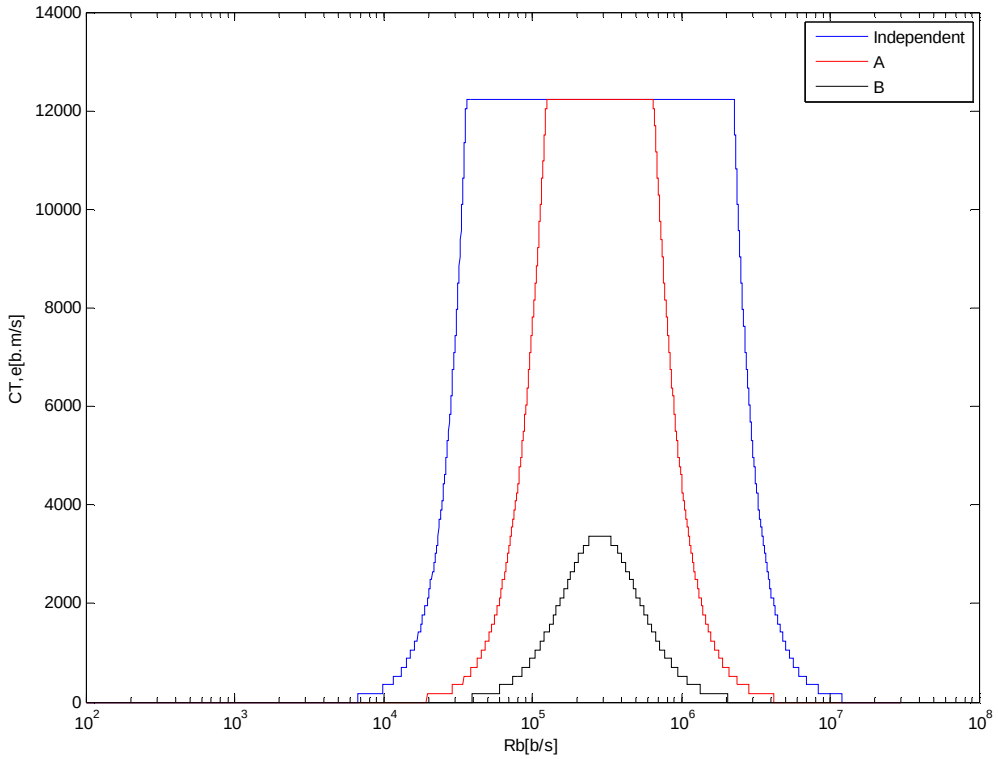

Fig.31 2-D Effective Transport Capacity versus Rb for 16-QAM modulation with 3 Rayleigh fading channels.

6. CONCLUSIONS AND FUTURE WORKS

6.1 Conclusions

In the first part of the thesis, the performance analysis of dispersed spectrum cognitive radio systems is conducted considering the effects of fading, number of dispersed bands, modulation, and coding. The symbol error probability is derived when each band undergoes independent and dependent Nakagami-m fading. Furthermore, the symbol error probability for both cases is extended to take the modulation effects into account. In addition, the effects of coding on symbol error probability performance are studied through computer simulations. Numerical results are presented to study the effects of fading, number of dispersed bands, modulation, and coding on the performance of dispersed spectrum cognitive radio systems. The results show that the effects of effects of fading, number of dispersed bands, modulation, and coding on the symbol error probability of dispersed spectrum cognitive radio systems is significant.

In the second part of this thesis, we have studied the relationship between the data rate and the effective transport capacity using specific modulation techniques, namely M-QAM, and M-PSK for ad hoc wireless networks based on MAC protocols. We have used the dispersed spectrum CR system with two different scenarios independent and dependent cases running over Nakagami-m fading channel for 3D configuration to enhance the performance in terms of effective transport capacity, which represents a realistic scenario of wireless sensor network.

6.2 Future Works

- This work can easily be extended to include variable transmit powers; each node transmits a different power, and then finding out the average power.
- Studying the performance of dispersed spectrum cognitive radio system from a different perspective, splitting the data into k segments, each one being carried over one band.
- The capacity of the ad hoc network was evaluated for the RESGO MAC protocol. It can be evaluated for other MAC protocols such as reserve-listen- and go (RESLGO) MAC protocol or reserve-choose-and-go (RESCHOGO) MAC protocol.
- Finding the effective transport capacity in the same scenario specified in this research but for with different types of node distributions.

REFERENCES

[1] J. Mitola and G. Q. Maguire, "Cognitive radio: Making software radios more personal," *IEEE Personal Commun. Mag.*, vol. 6, no. 4, pp. 13–18, August 1999.

[2] S. Gezici, H. Celebi, H. Vincent Poor, H. Arslan, "Fundamental limits on time delay estimation in dispersed spectrum cognitive radio systems," to appear in *IEEE Trans. on Wireless Communications*, 2008.

[3] S. Gezici, H. Celebi, H. Arslan, and H. V. Poor, "Theoretical limits on time delay estimation for ultra-wideband cognitive radios," *IEEE International Conference on UWB (ICUWB)*, vol. 2, Hannover, Germany, Sept. 2008, pp. 177–180.

[4] H. Celebi, K. A. Qaraqe, and H. Arslan, "Performance comparison of time delay estimation for whole and dispersed spectrum utilization methods in cognitive radio networks," *IEEE International Conference on Cognitive Radio Oriented Wireless Networks and Communications (CROWNCOM)*, Hannover, Germany, June 2009, pp. 1–6.

[5] G. Ferrari, B Baruffini, and O.K. Tonguz, "Spectral efficiency-connectivity. tradeoff in ad hoc wireless network," *Proc. International Symposium on Information Theory and Its Applications (ISITA)*, Parma, Italy, October 2004.

[6] G. Ferrari and O. K. Tonguz, "MAC protocols and transport capacity in ad hoc wireless networks: Aloha versus PR-CSMA," *Proc. IEEE Military Comm. Conf. (MILCOM)*, Boston, October 2003, vol. 2, pp. 1311-1318.

[7] O.K. Tonguz, and G. Ferrari, *Ad Hoc Wireless Networks: A Communication Theoretic Perspective*, New York: Wiley, 2006.

[8] P. Gupta and P. R. Kumar, "The capacity of wireless networks," *IEEE Trans. Inf. Theory*, vol. 46, no. 2, pp. 388–404, Mar. 2000.

[9] S. Meguerdichian, F. Koushanfar, M. Potkonjak, and M. Srivastava "Coverage problems in wireless ad-hoc sensor network," *Proc. IEEE INFOCOM*, pp. 1380-1387, 2001.

[10] S. Haykin, *Communication Systems*, 3rd ed., New York: Wiley, 1994.

[11] J.G. Proakis, *Digital Communications*, 3rd ed., New York: McGraw-Hill, 1995.

[12] J. Graig, "New simple and exact results for calculating the probability of error for two-dimensional signal constellation," *Proc. Milcom*, McLean, VA, pp. 571–575, Nov. 1991.

[13] A. Goldsmith, *Wireless Communications*, Cambridge: MIT Press, 2005.

[14] W.C. Y. Lee, *Mobile Communications: Design Fundamentals*, 2nd ed., New York: Wiley, 1993.

[15] I. Ghareeb, "Noncoherent MT-MFSK signals with diversity reception arbitrarily correlated and unbalanced Nakagami-m fading channel," *IEEE Journ. on Select. Areas in Commun*, vol. 23, pp. 1839-1850, Sep 2005.

[16] P. Elias, Coding for noisy Channel, *IRE Conv. Rec*., Part 4, pp. 37-46, 1955.

[17] J.M. Wozencraft and B. Reiffen, *Sequential Decoding*, Cambridge: MIT Press, 1961.

[18] J.L, Massey, *Threshold Decoding*, Cambridge: MIT Press, 1963.

[19] A. Dholakin, *Introduction to Convolutional Coding*, Dordrecht, The Netherlands: Kluwer Academic, 1994.

[20] L.H.C, Lee, *Convolutional Coding: Fundamentals and Applications*, Norwood, MA: Artech House, 1997.

[21] R. Johannesson and K.S Zigangirov, *Fundamentals of Convolutional Coding*, Piscatway, NJ: IEEE Press, 1999.

[22] S. Lin, and D. Castello, *Error Control Coding*, 2nd ed., New Jersey: Pearson Prentice Hall, 1983.

[23] S. Mason and H. Zimmermann, *Electronic Circuit, Signal, and System*, New York: Wiley, 1960.

[24] D. Pompili, T. Melodia, and I. Akyildiz, "Three-dimensional and two-dimensional deployment analysis of underwater acoustic sensor networks," *Ad Hoc Networks*, vol. 7, no. 4, pp. 778-790, June 2009.

[25] J. Hoydis, M. Petrova, and P. Mähönen, "Effects of topology on local throughput-capacity of ad hoc networks**,"** *Proc. of IEEE PIMRC,* Cannes, France, Sep. 2008.

[26] A. Chiganmi, K. Sarac, and R. Prakash, "Variable power broadcasting in ad hoc networks," *IEEE International Conference on Communication (ICC),* Istanbul, Turkey, June 2007, pp. 675-695.

[27] T. Chen, H. Zhang, G.M. Maggio and I. Chlamtac, "Topology management in CogMesh: A cluster-based cognitive radio mesh network," *Proc. IEEE ICC 2007 Workshop*, Glasgow, UK, June 24-28, 2007.

[28] P. Mähönen, M. Petrova, and J. Riihijärvi, “Applications of topology information for cognitive radios and networks,” *Proc. of IEEE Symposium on New Frontiers in Dynamic Spectrum Access Networks*, DySPAN, Dublin, Ireland, 2007, pp. 102-114.

[29] R. W. Thomas, R. S. Komali, L. A. DaSilva, and A. B. MacKenzie, “Joint power and channel minimization in topology control: A cognitive network approach,” *Proc. IEEE ICC 2007 Workshop*, Glasgow, UK, 2007. pp. 6538-6543.

VITA

Muneer Mohammad was born in Kuwait. He obtained a B.S. in electrical engineering from Jordan University of Science and Technology in January 2007 and an M.S. in electrical engineering from Texas A&M University in December, 2009. Before joining Texas A&M University as a Master's student, Mr. Mohammad worked as an engineer in Al-Hamad Construction Company. His research interests are in wireless communication, cognitive radio, frequency diversity, and its application to the ad hoc networks. Mr. Mohammad may be reached at: Department of Electrical and Computer Engineering, c\o Dr. Erchin Serpedin, Texas A&M University, College Station, TX 77843-3128. Mr. Mohammad's email address is: m.muneer@tamu.edu.